Check for updates

J. Fluid Mech. (2019), *vol.* 879, *pp.* 744–774. © Cambridge University Press 2019
doi:10.1017/jfm.2019.698

Viscous effects on the fundamental solution to ship waves

Hui Liang[1,†] **and Xiaobo Chen**[2,3,†]

[1]Technology Centre for Offshore and Marine, Singapore (TCOMS), 12 Prince Georges Park, 118411, Singapore

[2]Research Department, Bureau Veritas, 8 Cours du Triangle, Paris La Defense, 92937, France

[3]College of Shipbuilding Engineering, Harbin Engineering University, Harbin, 150001, China

(Received 3 December 2018; revised 31 July 2019; accepted 16 August 2019;
first published online 1 October 2019)

The fundamental solution to steady ship waves accounting for viscous effects (the viscous-ship-wave Green function) is investigated within the framework of the weakly damped free-surface flow theory. An explicit expression of the viscous-ship-wave Green function is firstly derived, and an accurate and efficient technique is described to evaluate the Green function via decomposing the free-surface term into the local-flow component and wave component. To delve into the physical features of the viscous-ship-wave Green function, the asymptotic approximations in the far field due to Kelvin, Havelock and Peters are presented for the flow-field point located inside, at and outside the Kelvin wedge. In addition, uniform approximations to the wave component based on the Chester–Friedman–Ursell (CFU) approximation and the Kelvin–Havelock–Peters (KHP) approximation are carried out. Both numerical evaluation and asymptotic approximations show that the singular behaviour is eliminated and the divergent waves associated with large wavenumbers leading to rapid oscillations are severely damped when viscous effects are accounted for. In addition, viscous effects also alter the apparent wake angle associated with the wave pattern created by a high-speed translating source, and the apparent wake angle is dependent on both $\mathscr{U}^{-1}$ and $\mathscr{U}^{-2}$, where $\mathscr{U}$ is the translating speed of the source.

Key words: surface gravity waves

1. Introduction

Waves accompanied by a steadily translating disturbance along a straight trajectory in calm water confined within a Kelvin wedge with a half-angle $\gamma_0 = 19°28'$ are of both theoretical and practical significance (Wehausen 1973). The stationary phase analysis to the dispersion relation shows that the open dispersion curve is divided by an inflexion into two branches corresponding to transverse waves and divergent waves, respectively (Lighthill 1978). Furthermore, more complicated ship waves are investigated, including nonlinear free-surface flows (Forbes 1989; Pethiyagoda, McCue & Moroney 2014*a*; Pethiyagoda *et al.* 2014*b*), the presence of shear current (Ellingsen

† Email addresses for correspondence: liang_hui@tcoms.sg, xiao-bo.chen@bureauveritas.com

https://doi.org/10.1017/jfm.2019.698 Published online by Cambridge University Press

2014; Li & Ellingsen 2016), the surface tension effect (Moisy & Rabaud 2014; Liang & Chen 2018), the bottom topography (Grue 2017), etc. The fundamental solution to this steady ship-wave problem (also referred to as the ship-wave Green function) represents the flow induced by a point source/sink with unit strength translating steadily along a rectilinear path in calm water, and it is an essential building block to constructing the boundary integral equation to represent the free-surface flow by a travelling ship hull within the linear potential theory (Brard 1972; Guével, Vaussy & Kobus 1974; Noblesse, Huang & Yang 2013). The expression of the ship-wave Green function in the form of a double Fourier integral is collected by Wehausen & Laitone (1960).

To evaluate the ship-wave Green function efficiently and with sufficient accuracy, the double Fourier integral is usually decomposed into a wave component dominant in the far field and a non-oscillatory local-flow component using Cauchy's residue theorem (Noblesse 1977, 1981; Newman 1987). The local-flow component expressed as a single integral of a complex exponential-integral function can be further approximated analytically (Noblesse *et al.* 2011). For the wave component, the asymptotic approximations due to Kelvin (1887), Havelock (1908) and Peters (1949) are applicable for the flow-field point located inside, at and outside the Kelvin wedge, respectively. Inside and at the cusp of the Kelvin wedge, waves decay as $R^{-1/2}$ and $R^{-1/3}$, respectively, where R is the horizontal distance from the disturbance, whereas waves decay exponentially outside the Kelvin wedge. Besides the approximations given by Kelvin, Havelock and Peters, Ursell (1960) gave an approximation associated with the Airy function and its derivative which is uniformly valid inside, at and outside the cusp, and he also reported the singular behaviour of waves generated by a concentrated pressure point. Ursell's approximation is based on an extension of the method of steepest descent which is also referred to as the Chester–Friedman–Ursell (CFU) approximation (Chester, Friedman & Ursell 1957). Lustri & Chapman (2013) studied the asymptotic behaviours at a low speed. Recently, Wu *et al.* (2018) proposed another alternative uniform approximation which combines the expressions given by Kelvin, Havelock and Peters, and thus it is referred to as the Kelvin–Havelock–Peters (KHP) approximation. Despite the fact that the KHP approximation is not as accurate as Ursell's approximation, yet it has a simple form consisting of elementary functions only, and it has been used to investigate the influence of the Froude number on the wave pattern (Wu *et al.* 2019). All of these efforts give an insight into the behaviours of the ship-wave Green function. Similar to the behaviours of waves generated by a pressure point (Ursell 1960), both numerical evaluation and asymptotic approximation show that very short and steep divergent waves exist when both source and flow-field points are on the free surface. Furthermore, the fundamental solution is singular as the flow-field point approaches the track of the source point (Clarisse & Newman 1994; Chen & Wu 2001; Motygin 2017). These unphysical behaviours partly stem from an ignorance of viscous effects.

Introducing viscous damping in water waves could be traced back to Lamb (1932). Longuet-Higgins (1992) assumed that the vortical boundary layer is attached to the free surface, and introduced the Helmholtz decomposition to divide the velocity into irrotational and vortical components. Joseph (2003) formulated the viscous potential flow equations for compressible fluids, and the phrase 'viscous potential flow' was proposed. Joseph & Wang (2004) developed a viscous corrected viscous potential flow theory, and investigated the decay rate of progressive gravity waves in comparison with Lamb's exact solution. Dias, Dyachenko & Zakharov (2008) made a systematic investigation into the effect of viscosity on free-surface waves in deep water, and a

https://doi.org/10.1017/jfm.2019.698 Published online by Cambridge University Press

weakly damped free-surface flow theory was established. However, their study made use of the streamfunction, and thus it is limited to the two-dimensional problem. Then, Dutykh & Dias (2007) generalized Dias *et al.*'s work to three dimensions, and a general joint Fourier–Laplace transform was applied to treat the governing equation and boundary conditions. However, it was suggested that the 'molecular' kinematic viscosity in the weakly damped free-surface flow $\nu = 1.0 \times 10^{-6}$ m^2 s^{-1} was too small, and it is typically taken as $\nu = 1.0 \times 10^{-4} \sim 1.0 \times 10^{-3}$ m^2 s^{-1} to account for the effective 'eddy' viscosity (Dias *et al.* 2008; Horsley & Forbes 2013).

In this paper, three-dimensional free-surface waves generated by a translating source with a constant speed, accounting for viscous effects are considered. The fluid is assumed to be incompressible, and the surface tension effect is disregarded. Viscous effects are accounted for based on the weakly damped free-surface flow theory (Dutykh & Dias 2007; Dias *et al.* 2008). The three-dimensional steady ship-wave problem accounting for viscous effects is pioneered by Cumberbatch (1965), and it shows that divergent waves are severely damped by viscous effects resulting in a finite wave amplitude along the track. Then, subsequent studies are carried out. Lu & Chwang (2005, 2007) studied the interfacial viscous ship waves in a system of two semi-infinite fluids with different densities, and asymptotic approximations valid in different flow regions are presented. Recently, Dai (2014) gave a uniform asymptotic expression for the interfacial viscous ship wave problem based on the CFU approximation (Chester *et al.* 1957).

Unlike existing studies and the authors' previous work (Liang & Chen 2018) in which the analysis of the pattern of iso-phase lines is conducted via phase relations, the emphasis of the present paper is placed on the influence of viscous effects on the amplitude of the fundamental solution for ship waves. Due to the presence of viscosity, the analysis becomes more complicated. Besides the technique to evaluate the double Fourier integral efficiently and accurately, five types of asymptotic approximations – including three classical non-uniform asymptotic approximations (Kelvin 1887; Havelock 1908; Peters 1949) and two uniform asymptotic approximations (CFU approximation (Chester *et al.* 1957) and KHP approximation (Wu *et al.* 2018)) – are made to obtain analytical expressions in the form of elementary functions. These analytical expressions explicitly reveal the underlying physics associated with the viscous-ship-wave Green function and illustrate how viscosity affects the amplitude of waves.

The layout of the paper is as follows. An explicit expression for the fundamental solution is first of all formulated in § 2, and the corresponding efficient and accurate evaluation method is described in § 3. To look into the flow physics of the viscous-ship-wave Green function, classical asymptotic approximations, which are valid inside, at and outside the Kelvin wedge due to Kelvin, Havelock and Peters, are used to convert the integral to algebraic expressions in § 4. The physical behaviour near the track is revealed. Due to the fact that Kelvin's and Peters' approximations are singular at the cusp, the uniform approximations based on the CFU approximation and KHP approximation are set forth in § 5. In § 6, numerical evaluation and asymptotic approximation of the viscous-ship-wave Green function are made and it is evident that the incorporation of viscous effects makes free-surface waves physically realistic – the singular behaviour is eliminated and rapid oscillations near the track due to divergent waves are severely damped. Then, in § 7, the apparent wake angle of free-surface waves generated by a translating source is investigated. It is demonstrated that the apparent wake angle is associated with both $\mathscr{U}^{-1}$ and $\mathscr{U}^{-2}$, where $\mathscr{U}$ is the travelling speed of the source. In addition, viscous effects widen the region near the track without divergent waves. Finally, conclusions drawn from the present study are summarized in § 8.

https://doi.org/10.1017/jfm.2019.698 Published online by Cambridge University Press

2. Viscous-ship-wave Green function

The viscous-ship-wave Green function is now considered. A frame of reference $OXYZ$ translating with the disturbance at a constant speed $\mathscr{U}$ in the direction of the negative X-axis is defined with the OXY plane coinciding with the undisturbed free surface and Z-axis orienting positively upward. Here, the translating speed $\mathscr{U}$ and the gravitational acceleration g are used to define the non-dimensional coordinates (x, y, z), and velocity potential ϕ with respect to $g/\mathscr{U}^2$ and $g/\mathscr{U}^3$, respectively. By starting from the linearized incompressible Navier–Stokes equations and applying the Helmholtz decomposition theorem, the linear free-surface boundary condition accounting for viscous effects can be obtained (for details refer to appendix A),

$$\frac{\partial^2\phi}{\partial x^2}+\frac{\partial\phi}{\partial z}+4\epsilon\frac{\partial^3\phi}{\partial x\partial z^2}=0, \quad \text{on } z=0, \tag{2.1}$$

where the non-dimensional parameter ϵ associated with viscous effects is defined as

$$\epsilon=g\nu/\mathscr{U}^3, \tag{2.2}$$

where ν denotes the kinematic fluid viscosity, and the molecular viscosity coefficient is $\nu=10^{-6}$ m^2 s^{-1}. Suppose that a source with strength σ is located at (ξ, η, ζ), and the corresponding potential is $\phi=\sigma G$, where G means the source potential with unit strength (also referred to as the Green function). The governing equation at a flow-field point (x, y, z) in the fluid domain for the unit source potential G beneath a free surface is

$$\nabla^2 G=\delta(x-\xi, y-\eta, z-\zeta), \quad \text{with } z\leqslant 0, \tag{2.3}$$

where δ means the Dirac delta function. The fundamental solution to the governing equation (2.3) satisfying the free-surface boundary condition (2.1) for the source potential can be expressed in the form of

$$4\pi G=-\frac{1}{r}+\frac{1}{r'}+G^F, \tag{2.4}$$

where r and r' are defined as

$$r=\sqrt{(x-\xi)^2+(y-\eta)^2+(z-\zeta)^2} \quad \text{and} \quad r'=\sqrt{(x-\xi)^2+(y-\eta)^2+(z+\zeta)^2}, \tag{2.5a,b}$$

and G^F denotes the potential due to the free-surface disturbance. Without loss of generality, we suppose that the source point is located at a point $(z\leqslant 0)$ along the z-axis which means that $\xi=0$ and $\eta=0$. In (2.4), expressions $1/r$ and $1/r'$ can be represented in the form of double Fourier integrals (Bronshtein *et al.* 2003)

$$\frac{1}{r}=\frac{1}{2\pi}\int_{-\infty}^{\infty}\int_{-\infty}^{\infty}\frac{1}{k}\mathrm{e}^{-k|z-\zeta|+\mathrm{i}(\alpha x+\beta y)}\,\mathrm{d}\alpha\,\mathrm{d}\beta, \tag{2.6a}$$

$$\frac{1}{r'}=\frac{1}{2\pi}\int_{-\infty}^{\infty}\int_{-\infty}^{\infty}\frac{1}{k}\mathrm{e}^{k(z+\zeta)+\mathrm{i}(\alpha x+\beta y)}\,\mathrm{d}\alpha\,\mathrm{d}\beta, \tag{2.6b}$$

on the (α, β) Fourier plane with $(\alpha, \beta)=k(\cos\theta, \sin\theta)$. By introducing the Fourier transform

$$\widetilde{G}(\alpha, \beta, z)=\int_{-\infty}^{\infty}\int_{-\infty}^{\infty}G(x, y, z)\mathrm{e}^{-\mathrm{i}(\alpha x+\beta y)}\,\mathrm{d}x\,\mathrm{d}y, \tag{2.7}$$

https://doi.org/10.1017/jfm.2019.698 Published online by Cambridge University Press

to the free-surface boundary condition given by (2.1) and the governing equation (2.3) as carried out in Liang & Chen (2017), we have

$$\widetilde{G}^F(\alpha,\beta,z)=A(\alpha,\beta)\mathrm{e}^{kz}, \tag{2.8a}$$

$$-2\pi\frac{\mathrm{e}^{-k|\zeta|}}{k}(-\alpha^2-k+4\mathrm{i}\epsilon\alpha k^2)+\left(2\pi\frac{\mathrm{e}^{k\zeta}}{k}+A\right)(-\alpha^2+k+4\mathrm{i}\epsilon\alpha k^2)=0. \tag{2.8b}$$

By making the inverse Fourier transform, we can obtain the free-surface term G^F in the form of

$$G^F=\frac{1}{\pi}\int_{-\infty}^{\infty}\int_{-\infty}^{\infty}\frac{1}{\mathscr{D}(\alpha,\beta)}\mathrm{e}^{k(z+\zeta)+\mathrm{i}(\alpha x+\beta y)}\,\mathrm{d}\alpha\,\mathrm{d}\beta, \tag{2.9}$$

where the denominator $\mathscr{D}$ in (2.9) represents the dispersion function associated with the linear free-surface boundary condition (2.1), and the dispersion functions on the $\alpha\beta$ and $k\theta$ Fourier planes are written as

$$\mathscr{D}(\alpha,\beta)=\alpha^2-\sqrt{\alpha^2+\beta^2}-4\mathrm{i}\epsilon\alpha(\alpha^2+\beta^2), \tag{2.10a}$$

$$\mathscr{D}(k,\theta)=k^2\cos^2\theta-k-4\mathrm{i}\epsilon k^3\cos\theta, \tag{2.10b}$$

with $(\alpha,\beta)=k(\cos\theta,\sin\theta)$. In (2.10), viscous effects only contribute to the imaginary part of the dispersion function. Hence, viscous effects do not affect the profile of the free-surface wave pattern, but will attenuate the amplitude of waves. Due to the fact that viscous effects are associated with k^3, they will have a tremendous influence on short waves with large wavenumbers. Then, expression (2.9) can be equivalently rewritten as

$$G^F=\frac{2}{\pi}\mathrm{Re}\int_{-\pi/2}^{\pi/2}\int_0^{\infty}\frac{1}{k\cos^2\theta-1-4\mathrm{i}\epsilon k^2\cos\theta}\mathrm{e}^{k(z+\zeta)+\mathrm{i}k(x\cos\theta+y\sin\theta)}\,\mathrm{d}k\,\mathrm{d}\theta. \tag{2.11}$$

By enforcing the dispersion equation $\mathscr{D}=0$, we get two characteristic wavenumbers

$$k_1=\frac{2}{\cos^2\theta+\sqrt{\cos^4\theta-16\mathrm{i}\epsilon\cos\theta}}=\frac{\cos^2\theta-\sqrt{\cos^4\theta-16\mathrm{i}\epsilon\cos\theta}}{8\mathrm{i}\epsilon\cos\theta}, \tag{2.12a}$$

$$k_2=\frac{\cos^2\theta+\sqrt{\cos^4\theta-16\mathrm{i}\epsilon\cos\theta}}{8\mathrm{i}\epsilon\cos\theta}. \tag{2.12b}$$

In the presence of viscous effects, the wavenumbers k_1 and k_2 are complex. Due to the fact that ϵ is a small parameter, the arguments of k_1 and k_2 are written as

$$\Lambda_1=\arctan\left(\frac{4\epsilon}{\cos^3\theta}\right)\quad\text{and}\quad\Lambda_2=-\pi+\arctan\left(\frac{\cos^3\theta}{4\epsilon}\right), \tag{2.13a,b}$$

which indicates that k_1 is located in the first quadrant, while k_2 is in the third quadrant of the Fourier plane as shown in figure 1.

https://doi.org/10.1017/jfm.2019.698 Published online by Cambridge University Press

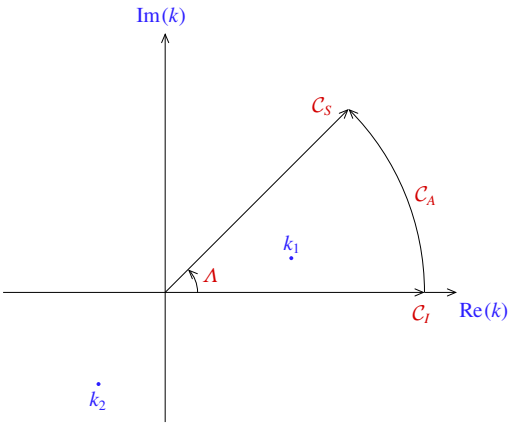


FIGURE 1. (Colour online) Sketch of deforming the integration path in the complex k-plane.

3. Decomposition of the Green function

For the purpose of evaluating the free-surface term G^F efficiently and accurately, it is usually decomposed into a non-oscillatory local-flow component and a wave component dominant in the far field. Here, we first of all decompose the free-surface term G^F into two components associated with characteristic wavenumbers k_1 and k_2, i.e.

$$G^F = G_1^F + G_2^F, \tag{3.1}$$

where G_1^F and G_2^F are expressed as

$$G_1^F = \frac{2}{\pi}\mathrm{Re}\int_{-\pi/2}^{\pi/2}\int_0^\infty \frac{1}{\sqrt{\cos^4\theta - 16\mathrm{i}\epsilon\cos\theta}}\frac{1}{k-k_1}\mathrm{e}^{k(z+\zeta)+\mathrm{i}k(x\cos\theta+y\sin\theta)}\,\mathrm{d}k\,\mathrm{d}\theta, \tag{3.2a}$$

$$G_2^F = -\frac{2}{\pi}\mathrm{Re}\int_{-\pi/2}^{\pi/2}\int_0^\infty \frac{1}{\sqrt{\cos^4\theta - 16\mathrm{i}\epsilon\cos\theta}}\frac{1}{k-k_2}\mathrm{e}^{k(z+\zeta)+\mathrm{i}k(x\cos\theta+y\sin\theta)}\,\mathrm{d}k\,\mathrm{d}\theta. \tag{3.2b}$$

To further decompose G_1^F and G_2^F given by (3.2), we consider the integration contour as illustrated in figure 1, the inner integral in (3.2) is the integration path $\mathcal{C}_I$ along the real k-axis. We may construct a closed contour including the integration path $\mathcal{C}_I$, an arc $\mathcal{C}_A$ with the radius $R\to\infty$ and a radial integration path designated by $\mathcal{C}_S$. It can be verified that the integral along $\mathcal{C}_A$ vanishes as the radius R tends to infinity. Besides, it is possible to find an argument Λ of the integration path $\mathcal{C}_S$ such that the exponent of the integrand is purely real, and this is the path that the integrand descends the most rapidly. Then, the argument of the steepest descent path Λ is expressed as

$$\Lambda = \arctan\left(-\frac{x\cos\theta + y\sin\theta}{z+\zeta}\right). \tag{3.3}$$

According to (2.13), the characteristic wavenumber k_1 is involved in the closed integration contour only when the argument of steepest descent path is larger than the argument of k_1, i.e. $\Lambda > \Lambda_1$. The other characteristic wavenumber k_2, however, is located in the third quadrant, and thus it can never be involved in the constructed

https://doi.org/10.1017/jfm.2019.698 Published online by Cambridge University Press

integration contour. Therefore, by applying Cauchy's residue theorem, the expression G_1^F in (3.2*a*) can be decomposed into a local-flow component G_1^L and a wave component dominant in the far field G_1^W associated with the integration patch $\mathcal{C}_S$ and the residue, respectively, i.e. $G_1^F = G_1^W + G_1^L$, while the representation G_2^F in (3.2*b*) only contributes to the local-flow component $G_2^F = G_2^L$. Furthermore, the integration along the steepest descent path $\mathcal{C}_S$ can be converted to the complex exponential-integral function as presented in appendix C. As a consequence, the wave component and local-flow component are given by

$$G^W = G_1^W = 4\,\mathrm{Re}\int_{-\pi/2}^{\pi/2} H(\Lambda-\Lambda_1)\frac{1}{\sqrt{\cos^4\theta - 16\mathrm{i}\epsilon\cos\theta}}\mathrm{i}\mathrm{e}^{k_1\mathcal{Z}}\,\mathrm{d}\theta, \tag{3.4}$$

and

$$G^L = G_1^L + G_2^L, \tag{3.5a}$$

with

$$G_1^L = \frac{2}{\pi}\mathrm{Re}\int_{-\pi/2}^{\pi/2}\frac{1}{\sqrt{\cos^4\theta - 16\mathrm{i}\epsilon\cos\theta}}\mathrm{e}^{k_1\mathcal{Z}}E_1(k_1\mathcal{Z})\,\mathrm{d}\theta, \tag{3.5b}$$

$$G_2^L = G_2^F = -\frac{2}{\pi}\mathrm{Re}\int_{-\pi/2}^{\pi/2}\frac{1}{\sqrt{\cos^4\theta - 16\mathrm{i}\epsilon\cos\theta}}\mathrm{e}^{k_2\mathcal{Z}}E_1(k_2\mathcal{Z})\,\mathrm{d}\theta, \tag{3.5c}$$

where $H(u)$ means the Heaviside function which equals 1 for $u>0$ and 0 otherwise, $\mathrm{e}^u E_1(u)$ denotes the complex exponential-integral function and $\mathcal{Z}$ is defined as

$$\mathcal{Z} = (z+\zeta) + \mathrm{i}(x\cos\theta + y\sin\theta). \tag{3.6}$$

By changing the integration path in the complex k-plane, the double Fourier integral is simplified to three single integrals given by (3.4) and (3.5), so that the free-surface term G^F can be efficiently evaluated. The gradients of the wave component and local-flow component are given by

$$\nabla G^W = 4\,\mathrm{Re}\int_{-\pi/2}^{\pi/2} H(\Lambda-\Lambda_1)\frac{\mathrm{i}k_1\mathrm{e}^{k_1\mathcal{Z}}}{\sqrt{\cos^4\theta - 16\mathrm{i}\epsilon\cos\theta}}\begin{Bmatrix}\mathrm{i}\cos\theta\\ \mathrm{i}\sin\theta\\ 1\end{Bmatrix}\mathrm{d}\theta, \tag{3.7a}$$

$$\nabla G^L = \frac{2}{\pi}\mathrm{Re}\int_{-\pi/2}^{\pi/2}\frac{k_1\mathrm{e}^{k_1\mathcal{Z}}E_1(k_1\mathcal{Z}) - k_2\mathrm{e}^{k_2\mathcal{Z}}E_1(k_2\mathcal{Z})}{\sqrt{\cos^4\theta - 16\mathrm{i}\epsilon\cos\theta}}\begin{Bmatrix}\mathrm{i}\cos\theta\\ \mathrm{i}\sin\theta\\ 1\end{Bmatrix}\mathrm{d}\theta, \tag{3.7b}$$

where the relation $\mathrm{d}\mathrm{e}^u E_1(u)/\mathrm{d}u = \mathrm{e}^u E_1(u) - 1/u$ has been used.

By applying the dynamic free-surface boundary condition, the free-surface elevation induced by the translating source is then expressed as

$$\mathcal{E} = -\frac{\partial G}{\partial x}\bigg|_{z=0} = -\frac{1}{4\pi}\frac{\partial G^F}{\partial x}\bigg|_{z=0} = \mathcal{E}^W + \mathcal{E}^L, \tag{3.8}$$

with

$$\mathcal{E}^W = \frac{1}{\pi}\mathrm{Re}\int_{-\pi/2}^{\pi/2} H(\Lambda-\Lambda_1)\frac{k_1\cos\theta\mathrm{e}^{k_1\mathcal{Z}}}{\sqrt{\cos^4\theta - 16\mathrm{i}\epsilon\cos\theta}}\,\mathrm{d}\theta, \tag{3.9a}$$

$$\mathcal{E}^L = -\frac{1}{2\pi^2}\mathrm{Re}\int_{-\pi/2}^{\pi/2}\mathrm{i}\cos\theta\frac{k_1\mathrm{e}^{k_1\mathcal{Z}}E_1(k_1\mathcal{Z}) - k_2\mathrm{e}^{k_2\mathcal{Z}}E_1(k_2\mathcal{Z})}{\sqrt{\cos^4\theta - 16\mathrm{i}\epsilon\cos\theta}}\,\mathrm{d}\theta. \tag{3.9b}$$

https://doi.org/10.1017/jfm.2019.698 Published online by Cambridge University Press

4. Asymptotic approximations

Despite § 3 enabling the efficient evaluation of the free-surface flow of a translating source by converting the double integral into two single integrals corresponding to the local-flow component and the wave component dominant in the far field, it is still difficult to obtain the intrinsic features of the viscous-ship-wave Green function from integral expressions (3.4) and (3.5). To delve into the physical features of the far-field waves, the asymptotic approximation is made to achieve an explicit analytical expression.

In this section, we make an asymptotic analysis of the free-surface term using Lighthill's two stage scheme (Lighthill 1960), which involves calculating the inner integral using Cauchy's residue theorem and the outer integral by means of the method of stationary phase or method of steepest descent (Wong 1989). Then, we use the form (2.9) given by

$$G^F = \frac{2}{\pi}\mathrm{Re}\int_{-\infty}^{\infty}\int_{0}^{\infty}\frac{1}{\alpha^2-\sqrt{\alpha^2+\beta^2}-4\mathrm{i}\epsilon\alpha(\alpha^2+\beta^2)}\mathrm{e}^{-\sqrt{\alpha^2+\beta^2}d+\mathrm{i}(\alpha x+\beta y)}\,\mathrm{d}\alpha\,\mathrm{d}\beta, \quad (4.1)$$

with $-d=z+\zeta\leqslant 0$. For a small ϵ, the root to the dispersion function (2.10*a*) requiring $\mathrm{Re}(\alpha)>0$ is expressed as follows (Lu & Chwang 2007):

$$\alpha(\beta)\approx a_0+\mathrm{i}\epsilon a_1, \quad (4.2)$$

where a_0 and a_1 are given by

$$a_0(\beta)=\sqrt{\frac{1+m}{2}} \quad \text{and} \quad a_1(\beta)=\frac{(m+1)^3}{2m}=\frac{4a_0^6}{2a_0^2-1}, \quad \text{with } m=\sqrt{1+4\beta^2}. \quad (4.3a,b)$$

Then, we can obtain the wave component dominant in the far field using Cauchy's residue theorem, i.e.

$$G^W\approx -4H(x)\mathrm{Im}\int_{-\infty}^{\infty}\sqrt{\frac{1+m}{2m^2}}\exp[-a_0^2d-\epsilon a_1x+\mathrm{i}(a_0x+\beta y)]\,\mathrm{d}\beta, \quad (4.4)$$

with errors of the order of $O(\epsilon)$. By performing the change of variable $m=2\kappa^2+1$, representation (4.4) becomes

$$G^W\approx -8H(x)\int_0^{\infty}\exp\left[-(1+\kappa^2)d+4\epsilon x\frac{(\kappa^2+1)^3}{2\kappa^2+1}\right]\sin A\cos B\,\mathrm{d}\kappa, \quad (4.5)$$

where A and B are defined as

$$A=x\sqrt{1+\kappa^2}=R\sqrt{1+\kappa^2}\cos\gamma, \quad (4.6a)$$

$$B=y\kappa\sqrt{1+\kappa^2}=R\kappa\sqrt{1+\kappa^2}\sin\gamma, \quad (4.6b)$$

with $(x,y)=R(\cos\gamma,\sin\gamma)$.

In the second stage, the single integral given by (4.4) is further simplified by means of the method of stationary phase or method of steepest descent which requires us to find stationary or saddle points of the phase function (Wong 1989). In the far field ($R\gg 1$), the phase function is highly oscillatory leading to substantial cancellation

https://doi.org/10.1017/jfm.2019.698 Published online by Cambridge University Press

which in turn results in the integral decaying rapidly except in the neighbourhood of stationary or saddle points. Then, representation (4.5) can be rewritten as

$$G^W \approx -4H(x)\mathrm{Im}\int_{-\infty}^{\infty}\exp\left[-(1+\kappa^2)d-4\epsilon x\frac{(\kappa^2+1)^3}{2\kappa^2+1}\right]\exp[\mathrm{i}(A-B)]\,\mathrm{d}\kappa,$$
$$= -4H(x)\mathrm{Im}\int_{-\infty}^{\infty}\mathcal{A}(\kappa)\exp[\mathrm{i}R\psi(\kappa,\gamma)]\,\mathrm{d}\kappa, \tag{4.7}$$

where $\mathcal{A}(\kappa)$ represents the amplitude function

$$\mathcal{A}(\kappa)=\exp\left[-(1+\kappa^2)d-4\epsilon x\frac{(\kappa^2+1)^3}{2\kappa^2+1}\right]. \tag{4.8}$$

Due to the fact that no stationary point exists in the phase function $\mathrm{e}^{\mathrm{i}(A+B)}$, there is no contribution in the far field. In (4.7), the phase function $\psi(\kappa,\gamma)$ is defined as

$$\psi(\kappa,\gamma)=\sqrt{1+\kappa^2}(\cos\gamma-\kappa\sin\gamma). \tag{4.9}$$

Stationary points require the vanishing of the first-order derivative of the phase function, i.e. $\psi'=0$, and they are given by

$$\kappa_-=\frac{\cot\gamma}{4}\left(1-\sqrt{1-8\tan^2\gamma}\right)\quad\text{and}\quad\kappa_+=\frac{\cot\gamma}{4}\left(1+\sqrt{1-8\tan^2\gamma}\right), \tag{4.10a,b}$$

where κ_- and κ_+ are associated with transverse waves and divergent waves, respectively. Representation (4.10) indicates that there are two different stationary points when the polar angle $|\gamma|$ is less than the cusp angle $\gamma_0=\arctan\sqrt{1/8}$. When $|\gamma|=\gamma_0$, two stationary points coalesce. As $|\gamma|>\gamma_0$, two stationary points become two complex saddle points which are a complex conjugate pair.

4.1. *Waves within the Kelvin wedge* $|\gamma|<\gamma_0$

When the azimuthal angle of the flow-field point $|\gamma|$ is less than the Kelvin angle γ_0, the phase function is purely real and thus Kelvin's method of stationary phase (Wong 1989) can be applied. Then, expression (4.7) mainly stems from the contribution of stationary points κ_- and κ_+, and it is simplified to

$$G^W \approx -4H(x)\sqrt{\frac{2\pi}{R|\psi_-''|}}\mathrm{Im}\left\{\mathcal{A}_-\exp\left[\mathrm{i}R\psi_-+\mathrm{sgn}(\psi_-'')\frac{\pi}{4}\right]\right\}$$
$$-4H(x)\sqrt{\frac{2\pi}{R|\psi_+''|}}\mathrm{Im}\left\{\mathcal{A}_+\exp\left[\mathrm{i}R\psi_++\mathrm{sgn}(\psi_+'')\frac{\pi}{4}\right]\right\}, \tag{4.11}$$

where 'prime' means differentiation with respect to the variable κ, $\psi_\pm=\psi(\kappa_\pm,\gamma)$, $\psi_\pm''=\partial^2\psi(\kappa_\pm,\gamma)/\partial\kappa^2$, $\mathcal{A}_\pm=\mathcal{A}(\kappa_\pm)$ and the second derivative of the phase function is given by

$$\psi''(\kappa,\gamma)=\frac{-2\kappa^3\sin\gamma-3\kappa\sin\gamma+\cos\gamma}{(1+\kappa^2)^{3/2}}. \tag{4.12}$$

At stationary points $\kappa=\kappa_\pm$, expression (4.12) is written as (Ursell 1960):

$$\psi_\pm''=\mp\frac{4}{\sqrt{3}}\frac{Q\sin\gamma}{\sqrt{(1\pm Q)(1\mp Q/3)}}, \tag{4.13}$$

where $Q=\sqrt{1-8\tan^2\gamma}$. In (4.11), the first term is associated with transverse waves, and the second one is with divergent waves. In addition, ψ_-'' is greater than zero, whereas ψ_+'' is less than zero.

https://doi.org/10.1017/jfm.2019.698 Published online by Cambridge University Press

4.2. *Behaviours near the singular axis*

Within the pure gravity wave theory, the ship-wave Green function is singular when both source and flow-field points are located on the free surface $d = 0$ and the flow-field point approaches the track of the disturbance $y = 0$ (Ursell 1960; Clarisse & Newman 1994; Chen & Wu 2001). The singular behaviour stems from the divergent waves corresponding to the open dispersion curve leading to $k \to \infty$.

We consider a flow-field point in the downstream close to the track of the disturbance $y = \varepsilon R > 0$ with ε being a small parameter $\varepsilon < 1$. This indicates that

$$\sin\gamma = \frac{y}{R} = \varepsilon \quad \text{and} \quad \cos\gamma = \frac{x}{R} \approx 1 - \frac{\varepsilon^2}{2}. \tag{4.14a,b}$$

Then, two stationary points given by (4.10) are approximately equal to

$$\kappa_- = \varepsilon + \frac{5}{2}\varepsilon^3 + O(\varepsilon^5) \quad \text{and} \quad \kappa_+ = \frac{1}{2\varepsilon} - \frac{5}{4}\varepsilon + O(\varepsilon^3). \tag{4.15a,b}$$

Accordingly, the phase function and its second derivative at stationary points are given by

$$\psi_- = 1 - \varepsilon^2 + O(\varepsilon^4) \quad \text{and} \quad \psi_+ = \frac{1}{4\varepsilon} + \frac{\varepsilon}{4} + O(\varepsilon^3), \tag{4.16a,b}$$

$$\psi_-'' \approx 1 - 5\varepsilon^2 + O(\varepsilon^4) \quad \text{and} \quad \psi_+'' \approx -2\varepsilon + 8\varepsilon^3 + O(\varepsilon^5). \tag{4.16c,d}$$

By introducing (4.15) and (4.16) into formulation (4.11), we have the expression for the asymptotic behaviour of the wave component near the singular axis

$$\begin{aligned} G^W \approx\ & -4H(x)\sqrt{\frac{2\pi}{R}}\exp[-4\epsilon x(1+\varepsilon^2)]\sin\left[R\left(1-\frac{\varepsilon^2}{2}\right)+\frac{\pi}{4}\right] \\ & -4H(x)\sqrt{\frac{\pi}{\varepsilon R}}\exp\left[-\epsilon x\left(\frac{1}{8\varepsilon^4}-\frac{5}{4}\right)\right]\sin\left(\frac{x^2+y^2}{4y}+\frac{y}{4}-\frac{\pi}{4}\right). \end{aligned} \tag{4.17}$$

Due to viscous effects, the wave component G^W given by (4.17) at $d = 0$ and $y \to 0$ is no longer singular. The divergent waves associated with large wavenumbers die away near the track ($y \to 0$). Besides, waves along the track of the disturbance decay with the distance in the form of $\mathrm{e}^{-4\epsilon x}/\sqrt{x}$ (the first term associated with transverse waves).

When viscous effects are ignored, the second expression in (4.17) associated with divergent waves is consistent with the asymptotic representation of the pure gravity ship-wave problem given by (Ursell 1960; Chen & Wu 2001)

$$G_0^W \approx -4H(x)\sqrt{\frac{\pi}{y}}\sin\left(\frac{x^2}{4y}+\frac{y}{2}-\frac{\pi}{4}\right), \tag{4.18}$$

which is singular at the track of the disturbance $y = 0$, and this singular behaviour is embedded in divergent waves.

https://doi.org/10.1017/jfm.2019.698 Published online by Cambridge University Press

4.3. *Waves at the cusp line* $|\gamma| = \gamma_0$

As the flow-field point is located at the cusp line of the Kelvin wedge, two stationary points coalesce

$$\kappa_- = \kappa_+ = \kappa_0 = \frac{\sqrt{2}}{2}, \tag{4.19}$$

and then we apply Havelock's approximation (Havelock 1908) by expanding the phase function $\psi(\kappa, \gamma_0)$ as

$$\psi(\kappa, \gamma_0) \approx \psi(\kappa_0, \gamma_0) + \tfrac{1}{6}\psi_0'''(\kappa - \kappa_0)^3 + \cdots, \tag{4.20}$$

where the third derivative of the phase function is

$$\psi_0''' = \psi'''(\kappa_0, \gamma_0) = \frac{-3\kappa_0 \cos\gamma_0 - 3\sin\gamma_0}{(1+\kappa_0^2)^{5/2}}. \tag{4.21}$$

Then, the asymptotic expression along the cusp line is written as

$$G^W \approx -4H(x)\mathrm{Im}\left[\frac{\Gamma(1/3)}{\sqrt{3}}\mathcal{A}_0 \exp(\mathrm{i}R\psi_0)\left(\frac{6}{R|\psi_0'''|}\right)^{1/3}\right], \tag{4.22}$$

where $\psi_0 = \psi(\kappa_0, \gamma_0)$, $\mathcal{A}_0 = \mathcal{A}(\kappa_0)$ and $\Gamma(\cdot)$ denotes the gamma function (Abramowitz & Stegun 1964).

4.4. *Waves outside the Kelvin wedge* $|\gamma| > \gamma_0$

When the flow-field point is located outside the Kelvin wedge $|\gamma| > \gamma_0$, two stationary points turn to two complex saddle points

$$\kappa_- = \frac{\cot\gamma}{4}(1 - \mathrm{i}\sqrt{8\tan^2\gamma - 1}) \quad \text{and} \quad \kappa_+ = \frac{\cot\gamma}{4}(1 + \mathrm{i}\sqrt{\tan^2\gamma - 1}). \tag{4.23a,b}$$

Then, Peters' approximation (Peters 1949) based on the method of steepest descent is applied. In the present problem, ψ_-'' and ψ_+'' are a complex conjugate pair with $\mathrm{Im}(\psi_-'') > 0$ and $\mathrm{Im}(\psi_+'') < 0$. By deforming the integration path, only the contribution of the saddle point κ_- matters. The phase function is written as

$$\psi_-'' = |\psi_-''|\mathrm{e}^{\mathrm{i}\alpha_-}, \tag{4.24}$$

where α_- denote the argument of ψ_-'' which is complex when $|\gamma| > \gamma_0$. Then, the approximation to the wave component G^W outside the Kelvin wedge is written as

$$G^W \approx -4H(x)\mathrm{Im}\left\{\sqrt{\frac{2\pi}{R|\psi_-''|}}\mathcal{A}_- \exp\left[\mathrm{i}R\psi_- + \mathrm{i}\left(\frac{\pi}{4} - \frac{\alpha_-}{2}\right)\right]\right\}. \tag{4.25}$$

5. Uniform asymptotic approximations

In § 4, non-uniform asymptotic approximations, which are valid inside, at and outside the Kelvin wedge originally given by Kelvin (1887), Havelock (1908) and Peters (1949), respectively, are presented. These three approximations are valid in the respective regions. In addition, Kelvin's and Peters' approximations are singular at the cusp, and thus the flow physics in the vicinity of the cusp cannot be well represented. Here, we are focused on the asymptotic approximations uniformly valid in the far field based on the CFU approximation (Chester *et al.* 1957) and the KHP approximation (Wu *et al.* 2018).

https://doi.org/10.1017/jfm.2019.698 Published online by Cambridge University Press

5.1. *CFU approximation*

The CFU approximation was originally proposed by Chester *et al.* (1957) and it has been applied by Ursell (1960) and Dai (2014) to study the pure gravity and interfacial ship waves generated by a concentrated pressure point. As an elegant method uniformly valid in the fluid domain, the CFU method is straightforward in principle, but it is complicated in practice due to the ambiguity of the multiple-value problem (Wong 1989). The CFU approximation is applied here to approximate the wave component (4.7), and the multiple-value problem, which is missing in Ursell (1960), is discussed.

Following Chester *et al.* (1957), the phase function is represented by a cubic polynomial in u

$$\psi(\kappa,\gamma) = -u^3/3 + p(\gamma)u + q(\gamma). \tag{5.1}$$

Differentiating the phase function given by (5.1) with respect to u yields

$$\frac{\partial\psi(\kappa,\gamma)}{\partial\kappa}\frac{\partial\kappa}{\partial u} = -u^2 + p(\gamma). \tag{5.2}$$

The left-hand side vanishes when $\kappa=\kappa_\pm$, so does the right-hand side when $u=\pm\sqrt{p}$. Here, κ and u are in one-to-one correspondence. Therefore, $\kappa=\kappa_+$ and $\kappa=\kappa_-$ correspond to $u=+\sqrt{p}$ and $u=-\sqrt{p}$, respectively. By substituting $\kappa=\kappa_\pm$ and $u=\pm\sqrt{p}$ into (5.1), we can obtain p and q (Ursell 1960)

$$p^{3/2} = \frac{3}{4}(\psi_+ - \psi_-) = \frac{3^{5/2}}{64}\frac{\cos^2\gamma}{\sin\gamma}(\mathscr{Q}_+ - \mathscr{Q}_-), \tag{5.3a}$$

$$q = -\frac{1}{2}(\psi_+ + \psi_-) = -\frac{3^{3/2}}{32}\frac{\cos^2\gamma}{\sin\gamma}(\mathscr{Q}_+ + \mathscr{Q}_-), \tag{5.3b}$$

where $\mathscr{Q}_+ = \sqrt{1+Q}(1-Q/3)^{3/2}$ and $\mathscr{Q}_- = \sqrt{1-Q}(1+Q/3)^{3/2}$. In (5.3*b*), q can be straightforwardly and uniquely determined. However, it is noted that p is not uniquely determined by (5.3*a*). In fact, there are three values of p. When $\gamma<\gamma_0$, the phase function is purely real, and thus p can be determined uniquely in this circumstance. When γ is larger than γ_0, $\psi(\kappa,\gamma)$ is complex at saddle points, and ψ_- and ψ_+ are a complex conjugate pair. In order to uniquely determine the value of p, we study the behaviour of the function p and q near the cusp line, and we consider $\varepsilon_- = \gamma_0 - \gamma \geqslant 0$. Then, Q can be expanded as

$$Q = \sqrt{1-8\tan^2(\gamma_0-\varepsilon_-)} \approx \tfrac{3}{2^{1/4}}\cdot\varepsilon_-^{1/2} - \tfrac{33}{16}\cdot 2^{1/4}\cdot\varepsilon_-^{3/2}, \tag{5.4}$$

and then p and q are written as

$$\begin{aligned} p &= \left[\tfrac{3^{5/2}}{64}\left(\tfrac{8}{3}+\tfrac{20}{3}\sqrt{2}\varepsilon_-+\cdots\right)\left(4\cdot 2^{1/4}\cdot\varepsilon_-^{3/2} - \tfrac{9}{4}\cdot 2^{3/4}\cdot\varepsilon_-^{5/2}+\cdots\right)\right]^{2/3} \\ &\approx \tfrac{3}{2^{1/2}}\cdot\varepsilon_- + O(\varepsilon_-^2), \end{aligned} \tag{5.5a}$$

$$q = -\tfrac{3^{3/2}}{32}\left(\tfrac{8}{3}+\tfrac{20}{3}\sqrt{2}\varepsilon_-+\cdots\right)(2-3\sqrt{2}\varepsilon_-+\cdots) \approx -\tfrac{3^{1/2}}{2} - \tfrac{3^{1/2}}{2^{1/2}}\cdot\varepsilon_- + O(\varepsilon_-^2). \tag{5.5b}$$

https://doi.org/10.1017/jfm.2019.698 Published online by Cambridge University Press

Therefore, near the cusp line, p and q have the following asymptotic expansions:

$$p \approx -\tfrac{3}{2^{1/2}}(\gamma-\gamma_0)+O[(\gamma-\gamma_0)^2], \tag{5.6a}$$

$$q \approx -\tfrac{3^{1/2}}{2}+\tfrac{3^{1/2}}{2^{1/2}}(\gamma-\gamma_0)+O[(\gamma-\gamma_0)^2]. \tag{5.6b}$$

When $\gamma>\gamma_0$, p must be consistent with the value inside and at the cusp, and hence p can be uniquely determined. So, we consider $\varepsilon_+=\gamma-\gamma_0>0$, and then $p^{3/2}$ in (5.3*a*) can be expanded into

$$p^{3/2} \approx -\tfrac{3^{3/2}}{2^{3/4}}\mathrm{i}\varepsilon_+^{3/2}+O(\varepsilon_+^{5/2}). \tag{5.7}$$

In (5.7), $-\mathrm{i}$ can be expressed as $\exp(-\mathrm{i}\pi/2+\mathrm{i}\cdot 2n\pi)$ with $n=0, 1, 2, \ldots$ leading to multiple values. Therefore, $(-\mathrm{i})^{2/3}$ has three values. Nevertheless, only one of them is physically realistic. According to the asymptotic relation given by (5.6*a*), n should be taken to be 1. As a consequence, the expression of p for $\gamma>\gamma_0$ is written as

$$p=-\left\{\frac{3^{5/2}}{64}\frac{\cos^2\gamma}{\sin\gamma}\mathrm{Im}[\mathscr{Q}_- -\mathscr{Q}_+]\right\}^{2/3}. \tag{5.8}$$

Then, the ultimate expression of p is written as

$$p=\begin{cases}[3(\psi_+-\psi_-)/4]^{2/3} & \gamma\leqslant\gamma_0,\\ -[3\mathrm{Im}(\psi_- -\psi_+)/4]^{2/3} & \gamma\geqslant\gamma_0.\end{cases} \tag{5.9}$$

To obtain the final asymptotic approximation, the amplitude function is represented by a Bleistein sequence (Wong 1989)

$$\mathcal{A}(\kappa)\frac{\partial\kappa}{\partial u}=a_0+b_0u+(u^2-p)\mathcal{H}, \tag{5.10}$$

where the last term on the right-hand side is associated with the high-order term, and it is disregarded here. To calculate the coefficients a_0 and b_0, we enforce (5.10) at two saddle points $\kappa=\kappa_\pm$ written as

$$\mathcal{A}_\pm\left(\frac{\partial\kappa}{\partial u}\right)_\pm=\mathcal{A}(\kappa_\pm)\left(\frac{\partial\kappa}{\partial u}\right)_{u=\pm\sqrt{p}}=a_0\pm\sqrt{p}b_0. \tag{5.11}$$

Then, we can obtain the coefficient a_0 and b_0

$$a_0=\begin{cases}\dfrac{1}{2}\left[\mathcal{A}_-\left(\dfrac{\partial\kappa}{\partial u}\right)_- +\mathcal{A}_+\left(\dfrac{\partial\kappa}{\partial u}\right)_+\right] & \gamma\neq\gamma_0,\\ \mathcal{A}_0\left(\dfrac{\partial\kappa}{\partial u}\right)_{u=0} & \gamma=\gamma_0,\end{cases} \tag{5.12a}$$

$$b_0=\begin{cases}\dfrac{1}{2\sqrt{p}}\left[\mathcal{A}_+\left(\dfrac{\partial\kappa}{\partial u}\right)_+ -\mathcal{A}_-\left(\dfrac{\partial\kappa}{\partial u}\right)_-\right] & \gamma\neq\gamma_0,\\ \mathcal{A}_0'\left(\dfrac{\partial\kappa}{\partial u}\right)_{u=0}^2+\mathcal{A}_0\left(\dfrac{\partial^2\kappa}{\partial u^2}\right)_{u=0} & \gamma=\gamma_0.\end{cases} \tag{5.12b}$$

To obtain the expression b_0 at $\gamma=\gamma_0$ given by (5.12*b*), the Bleistein sequence (5.10) is differentiated with respect to u at $u=0$. In (5.12), $\mathcal{A}(\kappa)$ is the amplitude

https://doi.org/10.1017/jfm.2019.698 Published online by Cambridge University Press

function, which is already known. Then, the task is to calculate derivatives $\partial\kappa/\partial u$ and $\partial^2\kappa/\partial u^2$. To calculate these derivatives in (5.12), we differentiate the phase function as well as the corresponding cubic polynomial given by (5.1) and enforcing the resultant expression at two saddle points $\kappa=\kappa_\pm$ gives rise to

$$\psi''\left(\frac{\partial\kappa}{\partial u}\right)^2+\psi'\frac{\partial^2\kappa}{\partial u^2}=-2u\quad\text{with }\kappa=\kappa_\pm\text{ and }u=\pm\sqrt{p}. \tag{5.13}$$

Then, $\partial\kappa/\partial u$ at two saddle points is expressed as

$$\left(\frac{\partial\kappa}{\partial u}\right)_\pm=\sqrt{\frac{\mp2\sqrt{p}}{\psi''_\pm}}=\sqrt{\frac{\sqrt{3}}{2}\frac{\sqrt{p}}{\sin\gamma}Q^{-1}(1\pm Q)^{1/2}(1\mp Q/3)^{1/2}}. \tag{5.14}$$

In this problem, $\psi''_->0$ and $\psi''_+<0$ when $\gamma<\gamma_0$. Hence, expression (5.14) is real. When $u=0$, we further differentiate (5.13) which yields

$$\psi'''\left(\frac{\partial\kappa}{\partial u}\right)^3+3\psi''\frac{\partial\kappa}{\partial u}\frac{\partial^2\kappa}{\partial u^2}+\psi'\frac{\partial^3\kappa}{\partial u^3}=-2. \tag{5.15}$$

At the cusp line $\gamma=\gamma_0$, we have $\kappa=\kappa_0$ and $u=0$ as well as $\psi'_0=\psi''_0=0$. Then, $\partial\kappa/\partial u$ becomes,

$$\left(\frac{\partial\kappa}{\partial u}\right)_0=\left(\frac{-2}{\psi'''_0}\right)^{1/3}=\sqrt{\frac{3}{2}}. \tag{5.16}$$

When $\gamma>\gamma_0$, there are two saddle points which are a complex conjugate pair, and the corresponding second derivatives are also a conjugate pair. So, $\psi''_\pm$ can be written as

$$\psi''_\pm=\Psi''\exp(\pm\mathrm{i}\alpha), \tag{5.17}$$

where Ψ'' is real and positive, and α is the argument of ψ''_+. Then, expression $\mathrm{d}\kappa/\mathrm{d}u$ for $\gamma>\gamma_0$ is written as

$$\left(\frac{\partial\kappa}{\partial u}\right)_\pm=\sqrt{\frac{2\sqrt{-p}}{\Psi''}}\exp\left\{\mp\mathrm{i}\left[\frac{\pi}{4}+\binom{m}{n}\pi+\frac{\alpha}{2}\right]\right\}\quad\text{with }m,n=0,1,2,\ldots. \tag{5.18}$$

Again, the multiple-value problem occurs. To determine it uniquely, we consider $\varepsilon_+=\gamma-\gamma_0>0$ once again, and $\psi''_\pm$ can be expanded as

$$\psi''_\pm=\mp\tfrac{2^{7/4}}{3^{1/2}}\mathrm{i}\cdot\varepsilon_+^{1/2}-\tfrac{2^{3/2}}{3^{1/2}}\cdot\varepsilon_++O(\varepsilon_+^{3/2}). \tag{5.19}$$

To be consistent with expression (5.16) when ε_+ approaches zero, m and n must be equal to zero, so that $\partial\kappa/\partial u$ is uniquely determined. So far, a_0 can be determined, and no multiple-value problem is suffered from. To determine b_0, one needs to evaluate $\partial^2\kappa/\partial u^2$. To achieve this goal, we further differentiate expression (5.15) with respect to u, and then $\partial^2\kappa/\partial u^2$ at the cusp line is written as

$$\left(\frac{\partial^2\kappa}{\partial u^2}\right)_{u=0}=-\frac{\psi''''_0}{6\psi'''_0}\left(\frac{-2}{\psi'''_0}\right)^{2/3}=\frac{\psi''''_0}{(-54^{1/5}\psi'''_0)^{5/3}}. \tag{5.20}$$

https://doi.org/10.1017/jfm.2019.698 Published online by Cambridge University Press

In Dai (2014), the power is wrongly written as 3/5. Once a_0 and b_0 are determined, the uniform approximation to the wave component can be expressed as (Chester *et al.* 1957)

$$G^W = -4\,\mathrm{Im}\left\{2\pi\exp(-\mathrm{i}Rq)\left[\frac{a_0}{R^{1/3}}\mathrm{Ai}(-R^{2/3}p)+\frac{\mathrm{i}b_0}{R^{2/3}}\mathrm{Ai}'(-R^{2/3}p)\right]\right\}, \tag{5.21}$$

where $\mathrm{Ai}(\cdot)$ and $\mathrm{Ai}'(\cdot)$ denote the Airy function and its derivative, respectively (Abramowitz & Stegun 1964).

5.2. *KHP approximation*

The KHP approximation developed by Wu *et al.* (2018) is based on the approximation to the Airy function $\mathrm{Ai}(u)$ and its derivative $\mathrm{Ai}'(u)$, which are oscillatory for $u<0$ and decay exponentially for $u>0$ (Abramowitz & Stegun 1964). Their asymptotic approximations are present for both $u<0$ and $u>0$. Nevertheless, the asymptotic approximations are invalid near $u=0$ (the asymptotic approximation of $\mathrm{Ai}(u)$ is infinite at $u=0$, while that of $\mathrm{Ai}'(u)$ at $u=0$ is equal to zero). To treat this issue, a blending function $\exp(-u^2)$ is introduced so that the Airy function and its derivative are uniformly approximated using the asymptotic expressions as well as the values of $\mathrm{Ai}(0)\approx 0.355$ and $\mathrm{Ai}'(0)\approx -0.259$.

Inspired by the approximation to the Airy function and its derivative, a uniform approximation to the wave component G^W can be obtained in the same manner through combining three classical approximations (Kelvin, Havelock and Peters) introduced in § 4. The blending factor u is thus determined via the CFU approximation containing both the Airy function and its derivative.

Then, following the work by Wu *et al.* (2018), the approximation combining expressions by Kelvin and Havelock is written as

$$\begin{aligned} G^W_{KHP} \;=\; & -4H(x)F^-_{KH}\mathrm{Im}\left[\mathcal{A}_-\exp\left(\mathrm{i}R\psi_- +\frac{\pi}{4}\right)\right] \\ & -4H(x)F^+_{KH}\mathrm{Im}\left[\mathcal{A}_+\exp\left(\mathrm{i}R\psi_+ -\frac{\pi}{4}\right)\right] \quad \text{for } \gamma\leqslant\gamma_0, \end{aligned} \tag{5.22}$$

where the function $F^{\pm}_{KH}$ combining both Kelvin's and Havelock's approximations is expressed as

$$F^{\pm}_{KH}=(1-\mu)\sqrt{\frac{2\pi}{R|\psi''_{\pm}|}}+\mu\frac{\Gamma(1/3)}{\sqrt{6}}\left(\frac{6}{R|\psi'''_0|}\right)^{1/3}, \tag{5.23}$$

with the blending function given by

$$\mu=\exp[-(-R^{2/3}p)^2]=\exp\{-[3R(\psi_+-\psi_-)/4]^{4/3}\}. \tag{5.24}$$

In (5.24), expression (5.9) has been applied. Representation (5.24) is uniformly valid for $\gamma\leqslant\gamma_0$, and it is consistent with Havelock's approximation at the cusp line $\gamma=\gamma_0$. In the same manner, a uniformly valid approximation for $\gamma\geqslant\gamma_0$ can be obtained by combining expressions (4.22) and (4.25) due to Havelock and Peters

$$G^W_{KHP}=-4H(x)\mathrm{Im}\left[F^-_{HP}\mathcal{A}_-\exp\left(\mathrm{i}R\psi_- +\mathrm{i}\frac{\pi}{4}\right)\right] \quad \text{for } \gamma\geqslant\gamma_0, \tag{5.25}$$

https://doi.org/10.1017/jfm.2019.698 Published online by Cambridge University Press

where the function F_{HP}^{-} is expressed as

$$F_{HP}^{-} = (1-\mu')\sqrt{\frac{2\pi}{R|\psi_-''|}}\exp\left(-\frac{\mathrm{i}\alpha}{2}\right) + \mu'\frac{(1-\mathrm{i})\Gamma(1/3)}{\sqrt{6}}\left(\frac{6}{R|\psi_0'''|}\right)^{1/3}. \tag{5.26}$$

According to expression (5.9), the blending function μ' in (5.26) is defined as

$$\mu' = \exp\{-[3R\mathrm{Im}(\psi_- - \psi_+)/4]^{4/3}\}. \tag{5.27}$$

As a consequence, the KHP approximation including (5.22) and (5.25), which are applicable for $\gamma \leqslant \gamma_0$ and $\gamma \geqslant \gamma_0$, respectively, is obtained. It is uniform in the entire fluid domain and is consistent with Havelock's approximation at the cusp line $\gamma = \gamma_0$.

5.3. *Comments on the CFU and KHP approximations*

In this section, the CFU and KHP approximations, which are uniformly valid in the flow field, are considered. The classical CFU approximation contains the Airy function and its derivative, while the KHP approximation contains elementary functions only, and is thus fully analytical. Although the KHP approximation is less accurate than the CFU approximation, as noted by Wu *et al.* (2018), yet the KHP approximation that results in explicit expressions facilitates the analysis of the flow physics associated with the viscous-ship-wave Green function. In addition, the KHP approximation provides a formal decomposition of ship waves into transverse and divergent waves from (5.22). This feature is favourable in the study of flow physics.

6. Results of the viscous-ship-wave Green function

6.1. *Numerical results*

The results based on the numerical evaluation of the viscous-ship-wave Green function are considered. Figures 2 and 3 depict the free-surface term G^F varying along a transverse cut in the downstream at $x = 10.0$ generated by a fully submerged source $d = 0.1$ and a slightly submerged source $d = 1.0 \times 10^{-5}$ with unit strength. The translating speed of the point source is $\mathscr{U} = 3.132$ m s^{-1}. Here, both the pure gravity ship-wave Green function and the viscous-ship-wave Green function are displayed. Besides, two different non-dimensional viscosity coefficients $\epsilon = 3.2 \times 10^{-7}$ and $\epsilon = 3.2 \times 10^{-5}$ corresponding to the kinematic fluid viscosities $\nu = 10^{-6}$ m^2 s^{-1} and $\nu = 10^{-4}$ m^2 s^{-1} are considered.

When the singularity is fully submerged $d = 0.1$, as shown in figure 2, viscous effects do not make a difference because there is no obvious difference between the three panels. As for a slightly submerged source $d = 1.0 \times 10^{-5}$, as exhibited in figure 3, the difference is evident. In the top panel, in which viscous effects are ignored, the free-surface term G^F is strongly oscillatory, and the wave height near the track $y = 0$ is very large. When only the molecular viscosity $\epsilon = 3.2 \times 10^{-7}$ is accounted for in the middle panel, waves are greatly damped, but rapid oscillations still exist. When the non-dimensional viscosity coefficient is taken to be $\epsilon = 3.2 \times 10^{-5}$ in the bottom panel, waves become very smooth and highly oscillatory behaviours are severely damped due to viscous effects. It is noted that viscous effects only attenuate the short waves near the track associated with large wavenumbers. In the region with a relatively large azimuthal angle where short waves do not appear, waves are merely affected by viscous effects.

https://doi.org/10.1017/jfm.2019.698 Published online by Cambridge University Press

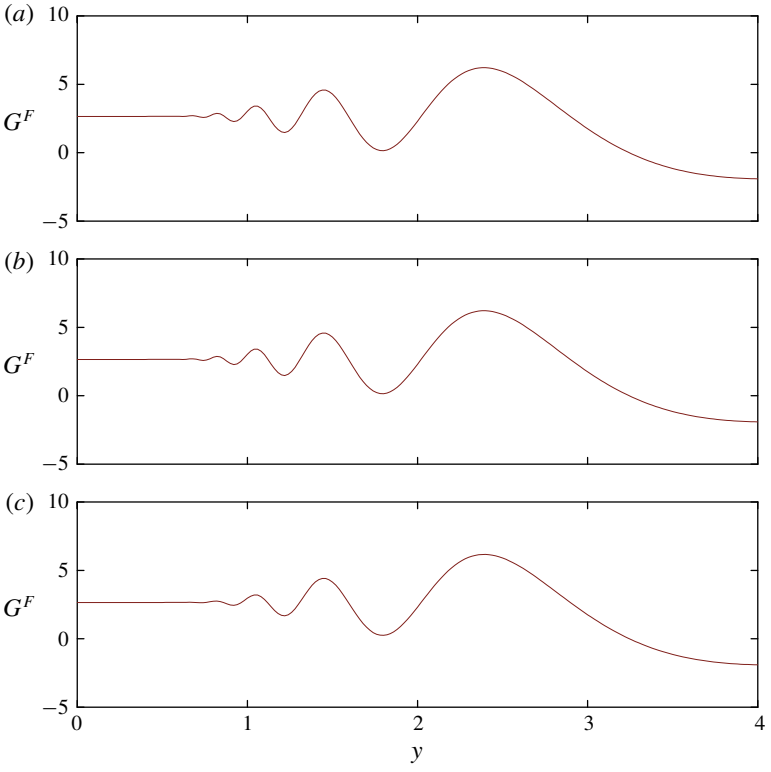


FIGURE 2. (Colour online) The free-surface term G^F induced by a source with the submergence $d = gD/\mathscr{U}^2 = 0.1$ and the translating speed $\mathscr{U} = 3.132$ m s^{-1} varying along a transverse cut at $x = gX/\mathscr{U}^2 = 10.0$. (*a*) Pure gravity ship-wave Green function; (*b*) viscous-ship-wave Green function with $\epsilon = 3.2 \times 10^{-7}$ corresponding to $\nu = 10^{-6}$ m^2 s^{-1}; (*c*) viscous-ship-wave Green function with $\epsilon = 3.2 \times 10^{-5}$ corresponding to $\nu = 10^{-4}$ m^2 s^{-1}.

6.2. *Non-uniform asymptotic approximations*

Then, we consider the asymptotic approximations to the wave component G^W due to Kelvin, Havelock and Peters as presented in § 4. For a flow-field point located inside ($|\gamma| < \gamma_0$), at ($|\gamma| = \gamma_0$) and outside ($|\gamma| > \gamma_0$) the Kelvin wedge, expressions (4.11), (4.22) and (4.25) are applied, respectively. Figure 4 shows the comparison between the numerical evaluation and three asymptotic approximations for a slightly submerged source with the submergence $d = 1.0 \times 10^{-5}$ and translating speed $\mathscr{U} = 3.132$ m s^{-1} considered in figure 3. Here, the numerical results are represented by solid lines, while the asymptotic approximations due to Kelvin, Havelock and Peters are plotted by dashed lines, hollow symbols and dash–dotted lines, respectively. The Kelvin's and Peters' expressions approximate the wave component G^W well when the azimuthal angle γ deviates from the cusp angle γ_0, and highly oscillatory behaviours of the pure gravity ship-wave Green function are well reflected by the Kelvin's approximation. At the cusp line, the approximations due to Kelvin and Peters are singular, whereas Havelock's approximation is well finite and agrees well with the numerical evaluation.

https://doi.org/10.1017/jfm.2019.698 Published online by Cambridge University Press

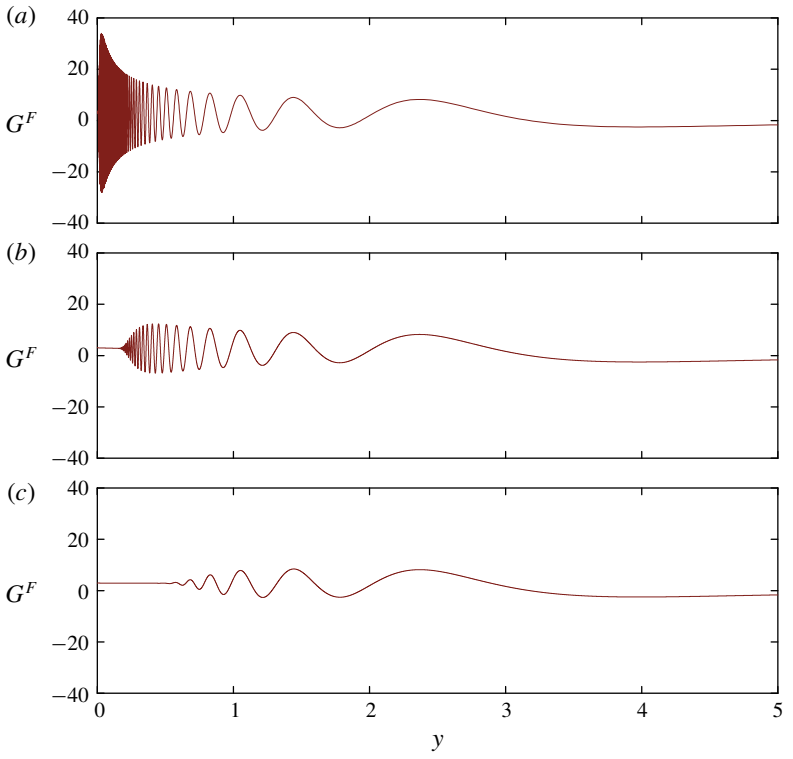


FIGURE 3. (Colour online) The free-surface term G^F induced by a slightly submerged source at $d = gD/\mathscr{U}^2 = 1.0 \times 10^{-5}$ and the forward speed $\mathscr{U} = 3.132$ m s^{-1} varying along a transverse cut at $x = gX/\mathscr{U}^2 = 10.0$. (*a*) Pure gravity ship-wave Green function; (*b*) viscous-ship-wave Green function with $\epsilon = 3.2 \times 10^{-7}$ corresponding to $\nu = 10^{-6}$ m^2 s^{-1}; (*c*) viscous-ship-wave Green function with $\epsilon = 3.2 \times 10^{-5}$ corresponding to $\nu = 10^{-4}$ m^2 s^{-1}.

6.3. *Uniform approximations*

Uniform approximations based on the CFU approximation and KHP approximation elucidated in § 5 are considered here. Figure 5 exhibits the wave component G^W induced by a slightly submerged translating source with the submergence $d = 1.0 \times 10^{-5}$ and translating speed $\mathscr{U} = 3.132$ m s^{-1} considered in figure 3. Results obtained from the CFU approximation and the KHP approximation are compared with the direct numerical evaluation. Generally, these three groups of results are in close agreement. Nevertheless, a slight difference is witnessed between the KHP approximation and the two others near the cusp line $\gamma = \gamma_0$. It has already been pointed out by Wu *et al.* (2018) that the KHP approximation is not as accurate as the CFU approximation in proximity to cusps. The KHP approximation is consistent with Havelock's expression at the cusp line. It is noted that the reminder of Havelock's approximation (4.22) is of the order of $O(R^{-2/3})$. However, the error of the CFU approximation is of the order of $O(R^{-4/3})$. Therefore, the CFU approximation is more accurate, but the accuracy of the KHP approximation can be improved by introducing high-order asymptotic expressions. The refined KHP approximation has been recently studied by Liang *et al.* (2020).

https://doi.org/10.1017/jfm.2019.698 Published online by Cambridge University Press

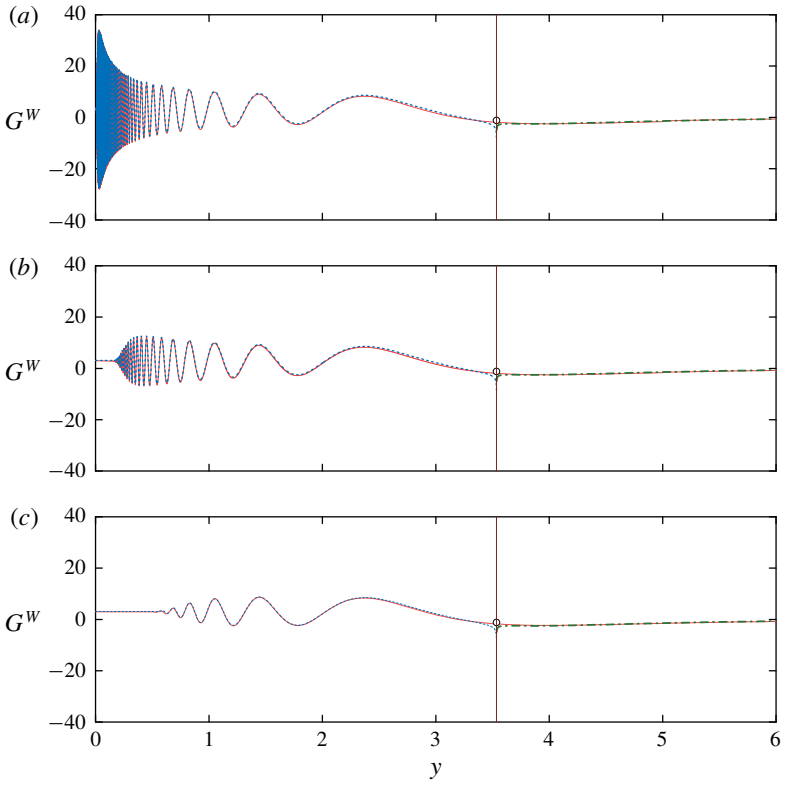


FIGURE 4. (Colour online) The wave component G^W induced by a slightly submerged source with the translating speed $\mathscr{U} = 3.132$ m s^{-1} at $d = 1.0 \times 10^{-5}$ varying along a transverse cut at $x = 10.0$. The comparison is made between the numerical evaluation by solid lines (——) and the asymptotic approximations due to Kelvin, Havelock and Peters represented by the dashed lines (– – – –), hollow scatters (○) and dash–dotted lines (– · – · –), respectively. (*a*) Pure gravity ship-wave Green function; (*b*) viscous-ship-wave Green function with $\epsilon = 3.2 \times 10^{-7}$; (*c*) viscous-ship-wave Green function with $\epsilon = 3.2 \times 10^{-5}$. The vertical line $y \approx 3.5$ corresponds to the cusp of Kelvin wedge.

Figure 6 depicts the wave component G^W induced by a source exactly located at the free surface $d = 0$ with the translating speed $\mathscr{U} = 3.132$ m s^{-1} varying along a transverse cut at $x = 10.0$. Besides the pure gravity ship-wave Green function, the viscous-ship-wave Green functions with viscosity coefficients $\epsilon = 3.2 \times 10^{-7}$ and $\epsilon = 3.2 \times 10^{-5}$ are exhibited. Results determined by the CFU approximation and KHP approximation are displayed in the top and bottom panels, respectively. It provides strong evidence that singular and highly oscillatory behaviours in the pure gravity ship-wave Green function are eliminated and damped by including viscous effects. Furthermore, steep short waves still exist if only molecular viscosity is accounted for, and can be largely removed via taking a proper viscosity coefficient, i.e. 100 times the molecular viscosity coefficient as suggested by Dias *et al.* (2008) and Horsley & Forbes (2013).

Figure 7 shows the plan view of the free-surface pattern generated by a steadily translating source with the submergence $d = 5.0 \times 10^{-2}$ and travelling speed $\mathscr{U} = 3.132$ m s^{-1} in a rectangular region $10 \leqslant x \leqslant 20$, $0 \leqslant y \leqslant 8$. Results obtained from

https://doi.org/10.1017/jfm.2019.698 Published online by Cambridge University Press

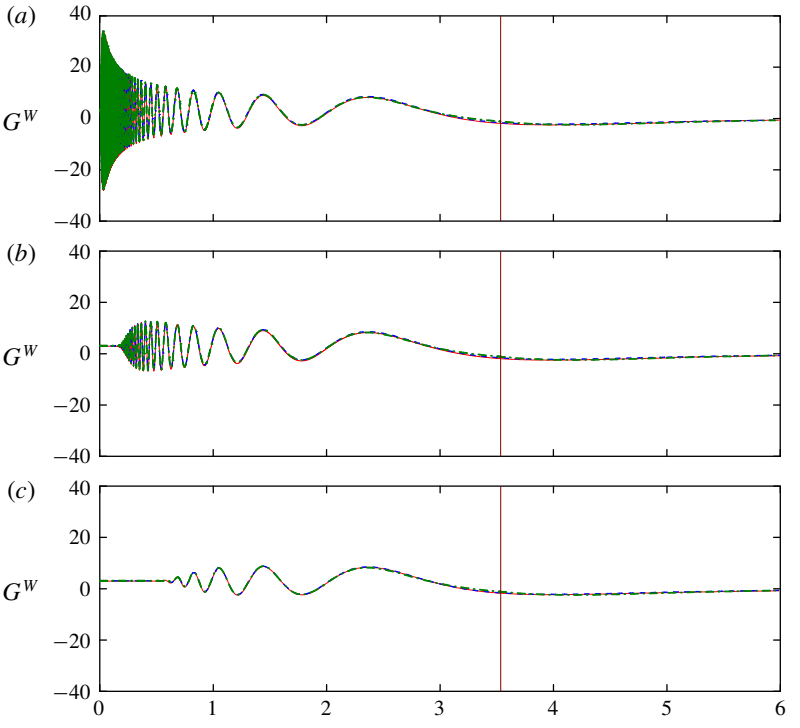


FIGURE 5. (Colour online) The wave component G^W induced by a slightly submerged source with the translating speed $\mathscr{U} = 3.132$ m s^{-1} at $d = gD/\mathscr{U}^2 = 1.0 \times 10^{-5}$ varying along a transverse cut at $x = gX/\mathscr{U}^2 = 10.0$. The comparison is made between the numerical evaluation by solid lines (——) and the uniform asymptotic approximations based on the CFU approximation by dashed lines (– – – –) and KHP approximation by dash-dotted lines (–·–·–). (*a*) Pure gravity ship-wave Green function; (*b*) viscous-ship-wave Green function with $\epsilon = 3.2 \times 10^{-7}$; (*c*) viscous-ship-wave Green function with $\epsilon = 3.2 \times 10^{-5}$. The vertical line $y \approx 3.5$ corresponds to the cusp of Kelvin wedge.

the numerical evaluation, the CFU approximation and KHP approximation are placed in the top row, centre row and bottom row, respectively. The pure gravity ship waves as well as viscous ship waves with the viscosity coefficients $\epsilon = 3.2 \times 10^{-7}$ and $\epsilon = 3.2 \times 10^{-5}$ are shown in the left column, middle column and right column, respectively. Discrepancies of wave patterns determined via three methods are indistinguishable. When viscous effects are ignored or only the molecular viscosity is accounted for, short waves are present inside the Kelvin wedge. In the right column in which the kinematic fluid viscosity coefficient is $\epsilon = 3.2 \times 10^{-5}$, short waves die out.

7. Apparent wake angle of waves by a point source

Inspired by observations by Rabaud & Moisy (2013), the investigation into the apparent wave angle of ship waves has been extensively carried out by considering the bow-stern interference effect (Noblesse *et al.* 2014) and a pressure patch with a smooth distribution (Benzaquen, Darmon & Raphaël 2014; Darmon, Benzaquen & Raphaël 2014; Miao & Liu 2015). Besides, as pointed out by Dias (2014), it is

https://doi.org/10.1017/jfm.2019.698 Published online by Cambridge University Press

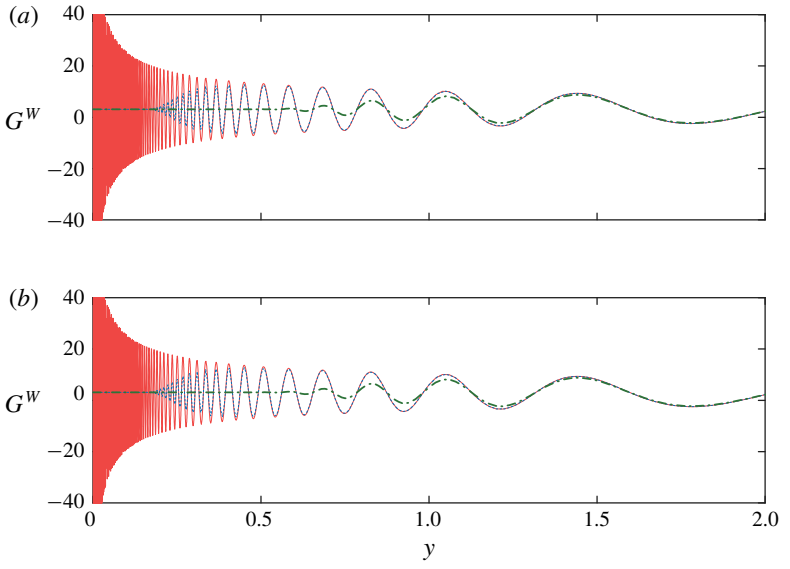


FIGURE 6. (Colour online) The wave component G^W induced by a source exactly at the free surface $d = gD/\mathscr{U}^2 = 0$ with the translating speed $\mathscr{U} = 3.132$ m s^{-1} varying along a transverse cut at $x = gX/\mathscr{U}^2 = 10.0$. Three groups of results are displayed including the pure gravity ship-wave Green function by solid lines (——), viscous-ship-wave Green functions with $\epsilon = 3.2 \times 10^{-7}$ ($\nu = 10^{-6}$ m^2 s^{-1}) plotted by dashed lines (– – – –) and $\epsilon = 3.2 \times 10^{-5}$ ($\nu = 10^{-4}$ m^2 s^{-1}) by dash-dotted lines (– · – · –). (*a*) CFU approximation; (*b*) KHP approximation.

important to focus on the amplitude. The subsequent study by Pethiyagoda *et al.* (2014*a*) demonstrates that even a point source can generate a wake with a smaller apparent angle than the Kelvin angle. Here, the apparent angle of waves associated with the viscous-ship-wave Green function is considered.

7.1. *Decomposition of transverse and divergent waves*

The uniform KHP approximation enables us to determine the individual contributions of transverse waves and divergent waves. Figure 8 shows the free-surface elevations induced by a translating source with the submergence $d = 0.01$ and the translating speed $\mathscr{U} = 3.132$ m s^{-1} varying with the ratio between the azimuthal angle and the Kelvin angle γ/γ_0 at a constant radius $R = 10$, and where the transverse waves and divergent waves are represented by solid lines and dashed lines, respectively. The envelope of divergent waves is also exhibited and is plotted by dash-dotted lines. In this case, the transverse waves with a small amplitude are mildly varying with the angle, but the divergent waves are oscillatory with an amplitude much higher than that of the transverse waves. Therefore, the divergent waves dominate the wave pattern at small d, corresponding to a small submergence or a high travelling speed. In addition, viscous effects hardly affect the transverse waves, but attenuate the amplitude of the divergent waves near the track. Furthermore, there is a narrow region near the track where the amplitude of divergent waves is almost zero when the source is submerged. The middle and bottom panels show that viscous effects make the region wider.

https://doi.org/10.1017/jfm.2019.698 Published online by Cambridge University Press

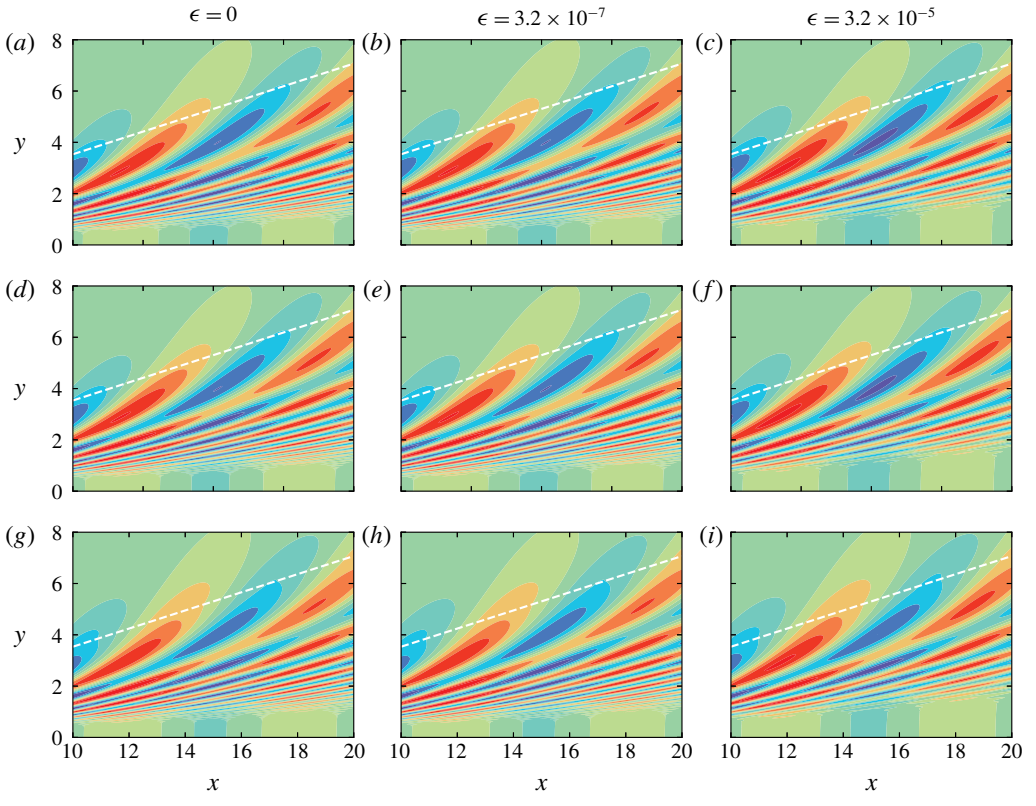


FIGURE 7. (Colour online) Plan view of the free-surface elevation generated by a steadily translating source with the submergence $d = gD/\mathscr{U}^2 = 5.0 \times 10^{-2}$ and the travelling speed $\mathscr{U} = 3.132$ m s^{-1}. Numerical evaluations are shown in (*a–c*), results determined by the CFU approximation in (*d–f*) and results by the KHP approximation in (*g–i*). Pure gravity ship waves as well as viscous ship waves with viscosity coefficients $\epsilon = 3.2 \times 10^{-7}$ and $\epsilon = 3.2 \times 10^{-5}$ corresponding to $\nu = 10^{-6}$ m^2 s^{-1} and $\nu = 10^{-4}$ m^2 s^{-1}, respectively, are placed from left to right. The white dashed line corresponds to the cusp of the Kelvin wedge.

7.2. *Apparent wake angle*

In order to study the apparent angle of free-surface waves generated by a translating source, the maximum of the envelope of divergent waves is considered. According to § 4.1, the envelope of divergent waves induced by a point source is

$$E = \frac{1}{\pi}\sqrt{1+\kappa_+^2}\,\exp\left[-(1+\kappa_+^2)d - 4\epsilon x\frac{(\kappa_+^2+1)^3}{2\kappa_+^2+1}\right]\sqrt{\frac{2\pi}{R|\psi_+''|}}, \tag{7.1}$$

where κ_+ and ψ_+'' are given by

$$\kappa_+ \approx \frac{1}{2\gamma} - \frac{7}{6}\gamma + O(\gamma^3) \quad \text{and} \quad \psi_+'' \approx -2\gamma + \frac{25}{3}\gamma^3 + O(\gamma^5), \tag{7.2a,b}$$

based on the small azimuthal angle approximation. Following Darmon *et al.* (2014), Pethiyagoda *et al.* (2014*a*), Miao & Liu (2015), the envelope of the divergent waves

https://doi.org/10.1017/jfm.2019.698 Published online by Cambridge University Press

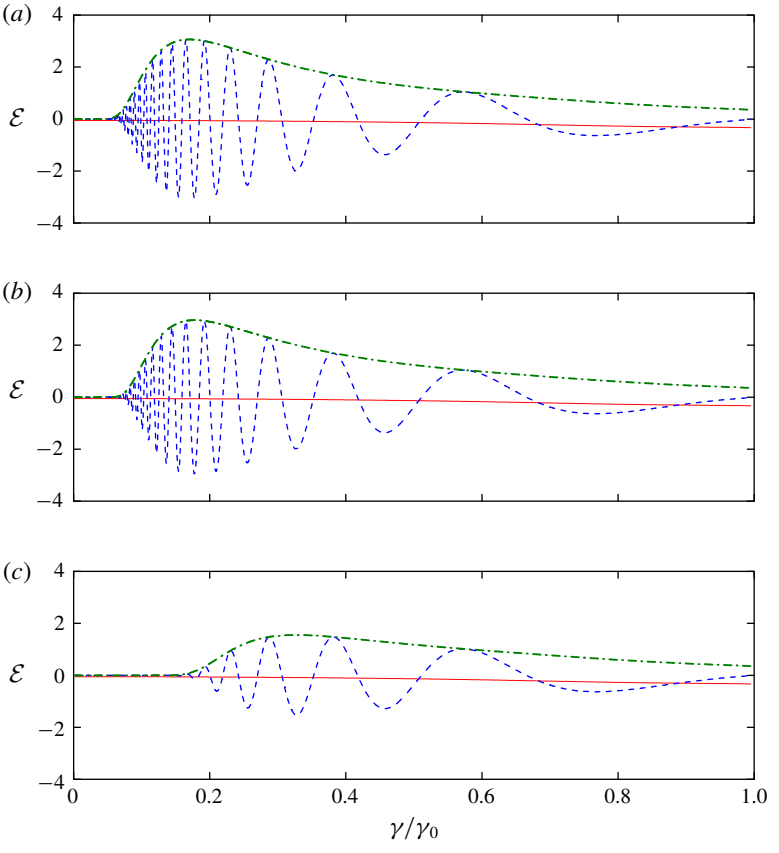


FIGURE 8. (Colour online) Decomposition of transverse and divergent waves inside the Kelvin wedge. The transverse waves are represented by solid lines (——), divergent waves by dashed lines (– – – –) and the envelope of divergent waves by dash-dotted lines (–·–·–). (*a*) Pure gravity ship waves; (*b*) viscous ship waves with $\epsilon = 3.2 \times 10^{-7}$; (*c*) viscous ship waves with $\epsilon = 3.2 \times 10^{-5}$.

is expanded as

$$E \approx \frac{1}{\sqrt{\pi R}}\left(\frac{1}{2}\gamma^{-3/2} + \frac{7}{8}\gamma^{1/2} + \cdots\right) \times \exp\left[-\frac{\epsilon x}{8}\gamma^{-4} - \left(\frac{\epsilon x}{12} + \frac{d}{4}\right)\gamma^{-2} + \frac{107}{180}\epsilon x + \frac{d}{6} + \cdots\right]. \tag{7.3}$$

By differentiating E with respect to γ and setting it to zero $\partial E/\partial\gamma = 0$, we can obtain the maximum wake angle subject to

$$\frac{\epsilon x}{2}\gamma^{-4} + \left(\frac{25}{24}\epsilon x + \frac{d}{2}\right)\gamma^{-2} - \frac{3}{2} = 0, \tag{7.4}$$

resulting in the apparent wake angle in a simple expression:

$$\gamma_{app} \approx \frac{1}{\sqrt{3}}\sqrt{d} + \frac{\sqrt{3}}{2}\frac{\epsilon x}{d^{3/2}} = \frac{\sqrt{gD}}{\sqrt{3}\mathscr{U}} + \frac{\sqrt{3}}{2}\frac{\nu X\sqrt{g}}{D^{3/2}\mathscr{U}^2}. \tag{7.5}$$

https://doi.org/10.1017/jfm.2019.698 Published online by Cambridge University Press

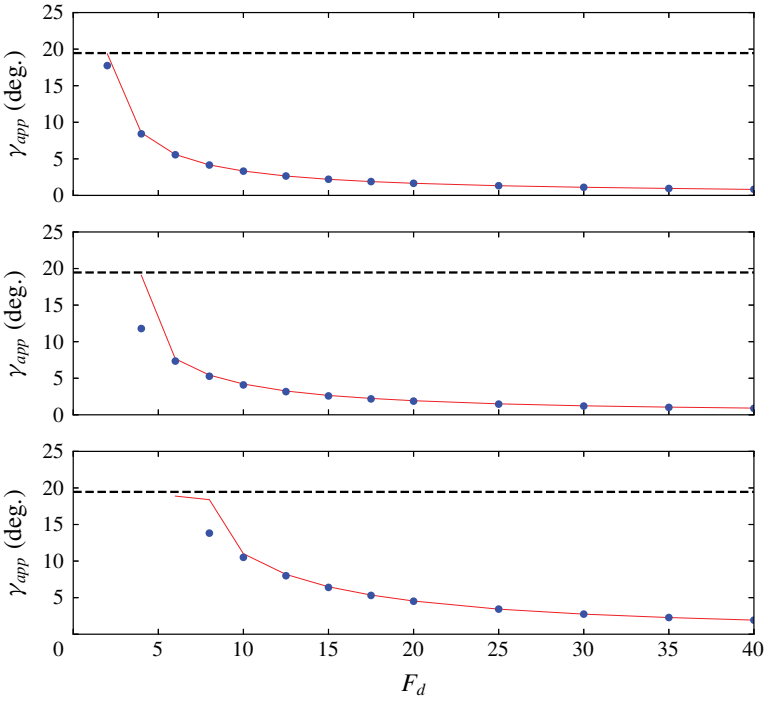


FIGURE 9. (Colour online) Apparent wake angle induced by a source with the submergence $D = 0.01$ m as a function of the submergence Froude number $F_d = \mathscr{U}/\sqrt{gD}$. The direct measurements are represented by solid lines, and the results determined by the asymptotic approximation (7.5) by solid symbols. The dashed line corresponds to the Kelvin angle.

When viscous effects are disregarded, expression (7.5) is consistent with the one given by Pethiyagoda *et al.* (2014*a*). Nevertheless, the apparent wake angle under the influence of viscous effects is dependent on the distance along the track from the point source, and it is associated with both $\mathscr{U}^{-1}$ and $\mathscr{U}^{-2}$. Furthermore, viscous effects play an increasingly important role with increasing distance. Figures 9 and 10 show the apparent wake angle induced by a translating source as a function of the submergence Froude number $F_d = \mathscr{U}/\sqrt{gD}$ at a fixed immersion depth $D = 0.01$ m and at a constant speed $\mathscr{U} = 31.3$ m s^{-1}. The asymptotic expression is exhibited by solid symbols, and the direct measurements are by solid lines. At a high submergence Froude number, viscous effects make a difference, and the apparent wake angle associated with viscous ship waves is larger than the pure gravity counterpart.

8. Concluding remarks

This paper presents a systematic study of the viscous-ship-wave Green function within the framework of weakly damped free-surface flows (Dias *et al.* 2008), and both numerical and analytical investigations are conducted. An explicit expression of the Green function in the form of a double Fourier integral is firstly formulated. Then, an efficient and accurate evaluation method is described by decomposing the free-surface term into a non-oscillatory local-flow component and a wave component dominant in the far field using Cauchy's residue theorem. To delve deeper into the

https://doi.org/10.1017/jfm.2019.698 Published online by Cambridge University Press

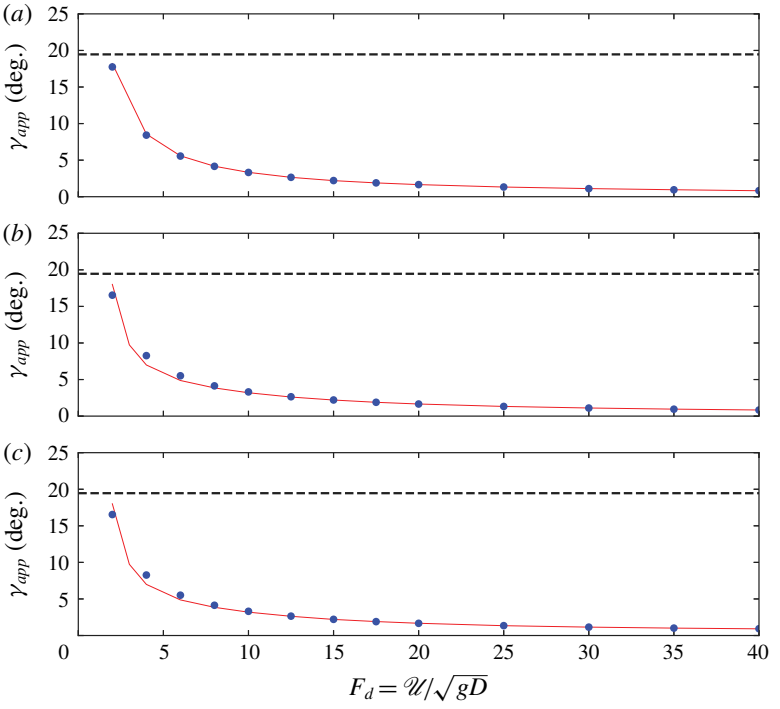


FIGURE 10. (Colour online) Apparent wake angle induced by a source at a constant speed $\mathscr{U} = 31.3$ m s^{-1} as a function of the submergence Froude number $F_d = \mathscr{U}/\sqrt{gD}$. The direct measurements are represented by solid lines, and the results determined by the asymptotic approximation (7.5) by solid symbols. The dashed line corresponds to the Kelvin angle.

flow physics of the viscous-ship-wave Green function, both non-uniform (Kelvin 1887; Havelock 1908; Peters 1949) and uniform asymptotic approximations (Chester *et al.* 1957; Wu *et al.* 2018) to far-field waves are made. Through this study, the following conclusions can be drawn:

(i) Viscous effects only contribute to the imaginary part of the dispersion function. Hence, they do not change the profile of the wave pattern, but will attenuate the amplitude of waves. The waves near the track associated with high wavenumbers are more susceptible to be influenced by viscous effects, and thus divergent waves are more severely damped. When the source is immersed, there is a narrow region near the cusp where the amplitude of divergent waves is almost zero. Viscous effects render this region wider.

(ii) Under the influence of viscous effects, the singular behaviour, which occurs in the pure gravity ship-wave Green function when both source and flow-field points are located on the free surface and the flow-field point approaches the track of the source point, is eliminated. If only the molecular viscosity $\nu = 1.0 \times 10^{-6}$ m^2 s^{-1} is taken, steep short waves are still present. As suggested by Dias *et al.* (2008) and Horsley & Forbes (2013), we take 100 times the molecular viscosity, i.e. $\nu = 1.0 \times 10^{-4}$ m^2 s^{-1}, and short waves to a large extent die out.

(iii) The KHP approximation provides a formal decomposition of transverse and divergent waves. At a high speed, the divergent waves dominate the wave pattern.

https://doi.org/10.1017/jfm.2019.698 Published online by Cambridge University Press

The apparent wake angle of free-surface waves generated by a translating source is dependent on viscous effects, and the apparent wake angle of viscous ship waves is larger than for pure gravity ship waves. Under the influence of viscous effects, the apparent wake angle is associated with both $\mathscr{U}^{-1}$ and $\mathscr{U}^{-2}$.

This study not only gives an insight into the influence of viscous effects on the fundamental solution to ship waves, but also provides a practical solution to removing non-physically singular and highly oscillatory behaviours embedded in the fundamental solution to ship waves.

Acknowledgements

The authors are grateful to Professor Y.-Z. Dai at Harbin Institute of Technology (Weihai, China) for kindly providing his unpublished notes to help authors to understand the CFU approximation. Constructive comments from three referees are highly appreciated. The second author has been partially supported by the National Natural Science Foundation of China (no. 51779054).

Appendix A. Free-surface boundary condition with viscous effects

This appendix reformulates the free-surface boundary condition accounting for viscous effects. It is assumed that the fluid is incompressible. Viscous effects are accounted for, but the surface tension effect is disregarded. The flow is governed by the continuity equation and the conservation of fluid momentum

$$\boldsymbol{\nabla}\cdot\boldsymbol{U}=0, \tag{A 1a}$$

$$\frac{\partial \boldsymbol{U}}{\partial T}=-\frac{1}{\rho}\boldsymbol{\nabla}P+\boldsymbol{\nabla}(-gZ)+\nu\nabla^2\boldsymbol{U}, \tag{A 1b}$$

where $\boldsymbol{U}=(U,V,W)$, T, ρ, P, g and ν represent the velocity components, time, fluid density, pressure, gravity acceleration and kinematic viscosity coefficient, respectively. Here, equation (A 1*b*) are the linearized Navier–Stokes equations with the advection term omitted.

On the free surface described by $Z=\Xi(X,Y,T)$, one kinematic boundary condition and two dynamic boundary conditions are satisfied (Dias *et al.* 2008)

$$\frac{\partial \Xi}{\partial T}=W,\quad \text{on } Z=0, \tag{A 2a}$$

$$\rho\nu\left(\frac{\partial U}{\partial Z}+\frac{\partial W}{\partial X}\right)=\rho\nu\left(\frac{\partial V}{\partial Z}+\frac{\partial W}{\partial Y}\right)=0,\quad \text{on } Z=0, \tag{A 2b}$$

$$P=P_a+2\rho\nu\frac{\partial W}{\partial Z},\quad \text{on } Z=0, \tag{A 2c}$$

where P_a is the atmospheric pressure. In accordance with the Helmholtz decomposition theorem, the velocity vector can be decomposed into curl-free and divergence-free components

$$\boldsymbol{U}=\boldsymbol{\nabla}\Psi+\boldsymbol{U}^T, \tag{A 3}$$

where the scalar function Ψ denotes the velocity potential in irrotational flow satisfying $\nabla^2\Psi=0$ and $\boldsymbol{U}^T=(U^T,V^T,W^T)$ represents the rotational flow. Substituting (A 3) into governing equations (A 1) yields

$$\nabla^2\Psi=\boldsymbol{\nabla}\cdot\boldsymbol{U}^T=0, \tag{A 4a}$$

$$\frac{\partial(\boldsymbol{\nabla}\Psi)}{\partial T}+\frac{\partial \boldsymbol{U}^T}{\partial T}=-\frac{1}{\rho}\boldsymbol{\nabla}P+\boldsymbol{\nabla}(-gZ)+\nu\nabla^2(\boldsymbol{\nabla}\Psi+\boldsymbol{U}^T). \tag{A 4b}$$

https://doi.org/10.1017/jfm.2019.698 Published online by Cambridge University Press

Taking the curl of (A 4*b*) gives rise to

$$\frac{\partial \Psi}{\partial T} + \frac{P - P_a}{\rho} + gZ = 0, \tag{A 5a}$$

$$\frac{\partial \boldsymbol{U}^T}{\partial T} = \nu \nabla^2 \boldsymbol{U}^T, \tag{A 5b}$$

where (A 5*a*) is known as the linear Bernoulli equation. Introducing (A 3) into the free-surface boundary conditions in (A 2) yields

$$\frac{\partial \Xi}{\partial T} = \frac{\partial \Psi}{\partial Z} + W^T, \quad \text{on } Z = 0, \tag{A 6a}$$

$$2\frac{\partial^2 \Psi}{\partial X \partial Z} + \frac{\partial U^T}{\partial Z} + \frac{\partial W^T}{\partial X} = 2\frac{\partial^2 \Psi}{\partial Y \partial Z} + \frac{\partial V^T}{\partial Z} + \frac{\partial W^T}{\partial Y} = 0, \quad \text{on } Z = 0, \tag{A 6b}$$

$$\frac{\partial \Psi}{\partial T} + g\Xi + 2\nu\left(\frac{\partial^2 \Psi}{\partial Z^2} + \frac{\partial W^T}{\partial Z}\right) = 0, \quad \text{on } Z = 0. \tag{A 6c}$$

Differentiating (A 6*c*) with respect to T and combining with (A 6*a*), we have

$$\frac{\partial^2 \Psi}{\partial T^2} + g\frac{\partial \Psi}{\partial Z} + gW^T + 2\nu\frac{\partial}{\partial T}\left(\frac{\partial^2 \Psi}{\partial Z^2} + \frac{\partial W^T}{\partial Z}\right) = 0, \quad \text{on } Z = 0. \tag{A 7}$$

According to the derivation presented in appendix B, we have the relation between Ξ and W^T

$$W^T = 2\nu\left(\frac{\partial^2 \Xi}{\partial X^2} + \frac{\partial^2 \Xi}{\partial Y^2}\right), \quad \text{on } Z = 0. \tag{A 8}$$

Substituting (A 6*c*) into (A 8), we have

$$W^T \approx 2\nu\left(\frac{\partial^2}{\partial X^2} + \frac{\partial^2}{\partial Y^2}\right)\left[-\frac{1}{g}\frac{\partial \Psi}{\partial T} - \frac{2\nu}{g}\left(\frac{\partial^2 \Psi}{\partial Z^2} + \frac{\partial W^T}{\partial Z}\right)\right] \approx \frac{2\nu}{g}\frac{\partial^3 \Psi}{\partial T \partial Z^2}, \quad \text{on } Z = 0, \tag{A 9}$$

where the quadratic terms associated with the viscosity are omitted. By inserting (A 9) into (A 7), we can obtain a new linear free-surface condition accounting for viscous effects

$$\frac{\partial^2 \Psi}{\partial T^2} + g\frac{\partial \Psi}{\partial Z} + 4\nu\frac{\partial^3 \Psi}{\partial T \partial Z^2} = 0, \quad \text{on } Z = 0, \tag{A 10}$$

where the Laplace equation $\nabla^2 \Psi = 0$ is applied. In a reference of frame steadily translating with a body, the potential is written as $\Psi = \mathscr{U} X + \Phi$, and then linear free-surface boundary condition becomes

$$\mathscr{U}^2\frac{\partial^2 \Phi}{\partial X^2} + g\frac{\partial \Phi}{\partial Z} + 4\nu\mathscr{U}\frac{\partial^3 \Phi}{\partial X \partial Z^2} = 0, \quad \text{on } Z = 0. \tag{A 11}$$

Appendix B. Proof of (A 8)

In Dutykh & Dias (2007), formulation (A 8) is obtained by means of the joint Laplace–Fourier transform. In this appendix, we derive it in a different way via

https://doi.org/10.1017/jfm.2019.698 Published online by Cambridge University Press

differentiating the free-surface boundary conditions. From the continuity equation given by (A 4*a*), we have

$$\frac{\partial U^T}{\partial X}+\frac{\partial V^T}{\partial Y}+\frac{\partial W^T}{\partial Z}=0. \tag{B 1}$$

Differentiating (B 1) with respect to Z yields

$$\frac{\partial^2 U^T}{\partial X\partial Z}+\frac{\partial^2 V^T}{\partial Y\partial Z}+\frac{\partial^2 W^T}{\partial Z^2}=0. \tag{B 2}$$

By calculating derivatives of the dynamic free-surface boundary condition (A 2*b*), we obtain the following two expressions

$$2\frac{\partial^3 \Psi}{\partial X^2\partial Z}+\frac{\partial^2 U^T}{\partial X\partial Z}+\frac{\partial^2 W^T}{\partial X^2}=0, \tag{B 3a}$$

$$2\frac{\partial^3 \Psi}{\partial Y^2\partial Z}+\frac{\partial^2 V^T}{\partial Y\partial Z}+\frac{\partial^2 W^T}{\partial Y^2}=0. \tag{B 3b}$$

Combining (B 2), (B 3*a*) and (B 3*b*) yields

$$2\left(\frac{\partial^3 \Psi}{\partial X^2\partial Z}+\frac{\partial^2 W^T}{\partial X^2}+\frac{\partial^3 \Psi}{\partial Y^2\partial Z}+\frac{\partial^2 W^T}{\partial Y^2}\right)=\frac{\partial^2 W^T}{\partial X^2}+\frac{\partial^2 W^T}{\partial Y^2}+\frac{\partial^2 W^T}{\partial Z^2}. \tag{B 4}$$

Considering (A 5*b*), we have

$$\frac{\partial W^T}{\partial T}=\nu\left(\frac{\partial^2 W^T}{\partial X^2}+\frac{\partial^2 W^T}{\partial Y^2}+\frac{\partial^2 W^T}{\partial Z^2}\right). \tag{B 5}$$

Inserting (B 4) into (B 5) yields

$$\frac{\partial W^T}{\partial T}=2\nu\left[\frac{\partial^2}{\partial X^2}\left(\frac{\partial \Psi}{\partial Z}+W^T\right)+\frac{\partial^2}{\partial Y^2}\left(\frac{\partial \Psi}{\partial Z}+W^T\right)\right]. \tag{B 6}$$

Accounting for the linearized kinematic free-surface boundary condition in (A 6*a*), we can eventually obtain the expression

$$W^T=2\nu\left(\frac{\partial^2 \Xi}{\partial X^2}+\frac{\partial^2 \Xi}{\partial Y^2}\right). \tag{B 7}$$

Appendix C. Exponential-integral function

Consider an integral in the form of

$$\mathcal{I}=\int_{\mathcal{C}_S}\frac{1}{k-K}\mathrm{e}^{k\mathcal{Z}}\,\mathrm{d}k, \tag{C 1}$$

where $\mathcal{C}_S$ denotes the integration path along which the exponent $k\mathcal{Z}$ is purely real so that the exponential function decays most rapidly, as described in figure 1. By

https://doi.org/10.1017/jfm.2019.698 Published online by Cambridge University Press

performing the change of variable $k = r(1 + \mathrm{i}\tan\Lambda)$ and $u = -r\mathcal{Z}(1 + \mathrm{i}\tan\Lambda)$, expression (C 1) becomes

$$\mathcal{I} = \int_0^\infty \frac{1}{r(1+\mathrm{i}\tan\Lambda) - K}(1+\mathrm{i}\tan\Lambda)\mathrm{e}^{r(1+\mathrm{i}\tan\Lambda)\mathcal{Z}}\,\mathrm{d}r = \int_0^\infty \frac{\mathcal{Z}}{u + K\mathcal{Z}}\frac{\mathrm{e}^{-u}}{\mathcal{Z}}\,\mathrm{d}u. \quad (C\,2)$$

Then, representation (C 2) can be further rewritten as

$$\mathcal{I} = \int_0^\infty \frac{\mathrm{e}^{-u}}{u + K\mathcal{Z}}\,\mathrm{d}u. \quad (C\,3)$$

The exponential-integral function is defined as follows (Abramowitz & Stegun 1964):

$$E_1(w) = \int_w^\infty \frac{\mathrm{e}^{-t}}{t}\,\mathrm{d}t. \quad (C\,4)$$

As a consequence, the integral given by (C 1) can be expressed as

$$\mathcal{I} = \mathrm{e}^{K\mathcal{Z}}E_1(K\mathcal{Z}). \quad (C\,5)$$

REFERENCES

Abramowitz, M. & Stegun, I. A. 1964 *Handbook of Mathematical Functions: with Formulas, Graphs, and Mathematical Tables*. National Bureau of Standards.

Benzaquen, M., Darmon, A. & Raphaël, E. 2014 Wake pattern and wave resistance for anisotropic moving disturbances. *Phys. Fluids* **26** (9), 092106.

Brard, R. 1972 The representation of a given ship form by singularity distributions when the boundary condition on the free surface is linearized. *J. Ship Res.* **16** (1), 79–92.

Bronshtein, I. N., Semendyayev, K. A., Musiol, G. & Muehlig, H. 2003 *Handbook of Mathematics*. Springer.

Chen, X. & Wu, G. X. 2001 On singular and highly oscillatory properties of the Green function for ship motions. *J. Fluid Mech.* **445** (1), 77–91.

Chester, C., Friedman, B. & Ursell, F. 1957 An extension of the method of steepest descents. *Math. Proc. Camb. Phil. Soc.* **53** (3), 599–611.

Clarisse, J. M. & Newman, J. N. 1994 Evaluation of the wave-resistance Green function. III: the single integral near the singular axis. *J. Ship Res.* **38** (1), 1–8.

Cumberbatch, E. 1965 Effects of viscosity on ship waves. *J. Fluid Mech.* **23** (3), 471–479.

Dai, Y. Z. 2014 On the interfacial viscous ship waves pattern. In *Proceeding of the 29th International Workshop on Water Waves and Floating Bodies, Osaka, Japan* (ed. M. Kashiwagi), pp. 25–28.

Darmon, A., Benzaquen, M. & Raphaël, E. 2014 Kelvin wake pattern at large Froude numbers. *J. Fluid Mech.* **738**, R3.

Dias, F. 2014 Ship waves and Kelvin. *J. Fluid Mech.* **746**, 1–4.

Dias, F., Dyachenko, A. I. & Zakharov, V. E. 2008 Theory of weakly damped free-surface flows: a new formulation based on potential flow solutions. *Phys. Lett.* A **372** (8), 1297–1302.

Dutykh, D. & Dias, F. 2007 Viscous potential free-surface flows in a fluid layer of finite depth. *C. R. Mathematique* **345** (2), 113–118.

Ellingsen, S. Å. 2014 Ship waves in the presence of uniform vorticity. *J. Fluid Mech.* **742**, R2.

Forbes, L. K. 1989 An algorithm for 3-dimensional free-surface problems in hydrodynamics. *J. Comput. Phys.* **82** (2), 330–347.

Grue, J. 2017 Ship generated mini-tsunamis. *J. Fluid Mech.* **816**, 142–166.

Guével, P., Vaussy, P. & Kobus, J. M. 1974 The distribution of singularities kinematically equivalent to a moving hull in the presence of a free surface. *Intl Shipbuild. Prog.* **21** (243), 311–324.

https://doi.org/10.1017/jfm.2019.698 Published online by Cambridge University Press

HAVELOCK, T. H. 1908 The propagation of groups of waves in dispersive media, with application to waves on water produced by a travelling disturbance. *Proc. R. Soc. Lond.* A **81** (549), 398–430.

HORSLEY, D. E. & FORBES, L. K. 2013 A spectral method for Faraday waves in rectangular tanks. *J. Engng Maths* **79** (1), 13–33.

JOSEPH, D. D. 2003 Viscous potential flow. *J. Fluid Mech.* **479**, 191–197.

JOSEPH, D. D. & WANG, J. 2004 The dissipation approximation and viscous potential flow. *J. Fluid Mech.* **505**, 365–377.

KELVIN, L. 1887 On the waves produced by a single impulse in water of any depth, or in a dispersive medium. *Proc. R. Soc. Lond.* A **42** (251–257), 80–83.

LAMB, H. 1932 *Hydrodynamics*. Cambridge University Press.

LI, Y. & ELLINGSEN, S. Å. 2016 Ship waves on uniform shear current at finite depth: wave resistance and critical velocity. *J. Fluid Mech.* **791**, 539–567.

LIANG, H. & CHEN, X. 2017 Capillary-gravity ship wave patterns. *J. Hydrodyn.* **29** (5), 825–830.

LIANG, H. & CHEN, X. 2018 Asymptotic analysis of capillary-gravity waves generated by a moving disturbance. *Eur. J. Mech. (*B*/Fluids)* **72**, 624–630.

LIANG, H., WU, H., HE, J. & NOBLESSE, F. 2020 Kelvin–Havelock–Peters approximations to a classical generic wave integral. *Appl. Math. Model.* **77**, 950–962.

LIGHTHILL, M. J. 1960 Studies on magneto-hydrodynamic waves and other anisotropic wave motions. *Phil. Trans.* A *Math. Phys. Engng Sci.* **252**, 397–430.

LIGHTHILL, M. J. 1978 *Waves in Fluids*. Cambridge University Press.

LONGUET-HIGGINS, M. S. 1992 Theory of weakly damped Stokes waves: a new formulation and its physical interpretation. *J. Fluid Mech.* **235**, 319–324.

LU, D.-Q. & CHWANG, A. T. 2005 Interfacial waves due to a singularity in a system of two semi-infinite fluids. *Phys. Fluids* **17** (10), 102107.

LU, D.-Q. & CHWANG, A. T. 2007 Interfacial viscous ship waves near the cusp lines. *Wave Motion* **44** (7–8), 563–572.

LUSTRI, C. J. & CHAPMAN, S. J. 2013 Steady gravity waves due to a submerged source. *J. Fluid Mech.* **732**, 660–686.

MIAO, S. & LIU, Y. 2015 Wave pattern in the wake of an arbitrary moving surface pressure disturbance. *Phys. Fluids* **27** (12), 122102.

MOISY, F. & RABAUD, M. 2014 Mach-like capillary-gravity wakes. *Phys. Rev.* E **90** (2), 023009.

MOTYGIN, O. V. 2017 Numerical approximation of oscillatory integrals of the linear ship wave theory. *Appl. Numer. Maths* **115**, 99–113.

NEWMAN, J. N. 1987 Evaluation of the wave-resistance Green function. I: the double integral. *J. Ship Res.* **31** (2), 79–90.

NOBLESSE, F. 1977 The fundamental solution in the theory of steady motion of a ship. *J. Ship Res.* **21** (2), 82–88.

NOBLESSE, F. 1981 Alternative integral representations for the Green function of the theory of ship wave resistance. *J. Engng Maths* **15** (4), 241–265.

NOBLESSE, F., DELHOMMEAU, G., HUANG, F. & YANG, C. 2011 Practical mathematical representation of the flow due to a distribution of sources on a steadily advancing ship hull. *J. Engng Maths* **71** (4), 367–392.

NOBLESSE, F., HE, J., ZHU, Y., HONG, L., ZHANG, C., ZHU, R. & YANG, C. 2014 Why can ship wakes appear narrower than Kelvin's angle? *Eur. J. Mech. (*B*/Fluids)* **46**, 164–171.

NOBLESSE, F., HUANG, F. & YANG, C. 2013 The Neumann–Michell theory of ship waves. *J. Engng Maths* **79** (1), 51–71.

PETERS, A. S. 1949 A new treatment of the ship wave problem. *Commun. Pure Appl. Maths* **2** (2–3), 123–148.

PETHIYAGODA, R., MCCUE, S. W. & MORONEY, T. J. 2014*a* What is the apparent angle of a Kelvin ship wave pattern? *J. Fluid Mech.* **758**, 468–485.

PETHIYAGODA, R., MCCUE, S. W., MORONEY, T. J. & BACK, J. M. 2014*b* Jacobian-free Newton–Krylov methods with GPU acceleration for computing nonlinear ship wave patterns. *J. Comput. Phys.* **269**, 297–313.

https://doi.org/10.1017/jfm.2019.698 Published online by Cambridge University Press

RABAUD, M. & MOISY, F. 2013 Ship wakes: Kelvin or Mach angle? *Phys. Rev. Lett.* **110** (21), 214503.

URSELL, F. 1960 On Kelvin's ship-wave pattern. *J. Fluid Mech.* **8** (03), 418–431.

WEHAUSEN, J. V. 1973 The wave resistance of ships. *Adv. Appl. Mech.* **13**, 93–245.

WEHAUSEN, J. V. & LAITONE, E. V. 1960 Surface waves. *Hanbuch der Physik* **9**, 446–778.

WONG, R. 1989 *Asymptotic Approximations of Integrals*. Academic Press.

WU, H., HE, J., LIANG, H. & NOBLESSE, F. 2019 Influence of Froude number and submergence depth on wave patterns. *Eur. J. Mech. (*B*/Fluids)* **75**, 258–270.

WU, H., HE, J., ZHU, Y. & NOBLESSE, F. 2018 The Kelvin–Havelock–Peters farfield approximation to ship waves. *Eur. J. Mech. (*B*/Fluids)* **70**, 93–101.

https://doi.org/10.1017/jfm.2019.698 Published online by Cambridge University Press